Journal of Medicinal Chemistry

pubs.acs.org/jmc

Article

Reinvent Aliphatic Arsenicals as Reversible Covalent Warheads toward Targeted Kinase Inhibition and Non-acute Promyelocytic Leukemia Cancer Treatment

Yang Zhao, Xinyue Zhao, Lewei Duan, Ruxue Hou, Yuxin Gu, Zhen Liu, Jianbin Chen, Feizhen Wu, Limin Yang, X. Chris Le, Qiuquan Wang, and Xiaowen Yan*

Cite This: J. Med. Chem. 2024, 67, 5458−5472

Read Online

ACCESS | Metrics & More | Article Recommendations | Supporting Information

ABSTRACT: The success of arsenic in acute promyelocytic leukemia (APL) treatment is hardly transferred to non-APL cancers, mainly due to the low selectivity and weak binding affinity of traditional arsenicals to oncoproteins critical for cancer survival. We present herein the reinvention of aliphatic trivalent arsenicals (As) as reversible covalent warheads of As-based targeting inhibitors toward Bruton's tyrosine kinase (BTK). The effects of As warheads' valency, thiol protection, methylation, spacer length, and size on inhibitors' activity were studied. We found that, in contrast to the bulky and rigid aromatic As warhead, the flexible aliphatic As warheads were well compatible with the well-optimized guiding group to achieve nanomolar inhibition against BTK. The optimized As inhibitors effectively blocked the BTK-mediated oncogenic signaling pathway, leading to elevated antiproliferative activities toward lymphoma cells and xenograft tumor. Our study provides a promising strategy enabling rational design of new aliphatic arsenic-based reversible covalent inhibitors toward non-APL cancer treatment.

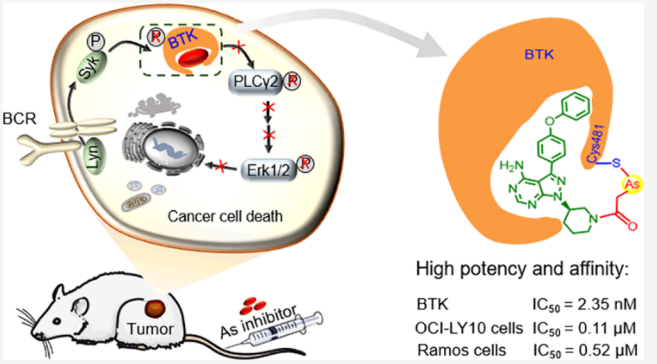

INTRODUCTION

Arsenicals such as realgar (As_4S_4), orpiment (As_2S_3), and arsenic trioxide (ATO) are ancient medicines used for the treatment of various diseases for more than two thousand years.[1,2] Besides inorganic species, organic arsenicals are also created and tested for medical use. Salvarsan (Figure 1A), an organic aromatic arsenical recognized as the first modern antimicrobial drug, had long been introduced at the beginning of the 1910s as the most common remedy for syphilis.[3,4] Since then, organic arsenicals, including melarsoprol[5] and GSAO[6] that contain phenylarsonous acid (Figure 1A), as well as MER1[7] and darinaparsin[8] that comprise a dimethylarsinous acid, together with different arsenical drug delivery agents,[9−11] have been tested for cancer and other disease treatment. However, along with the incidence of serious toxic and side effects, the application of arsenic in medicine gradually declined.[12]

The value of arsenic-based drugs attracts renewed attention owing to the successful application of ATO in clinical treatment of acute promyelocytic leukemia (APL).[13] In contrast to most other blood malignancies, PML-RARα fusion oncoprotein was regarded as the driver of APL.[14] The underlying molecular mechanism of ATO-induced APL cell death was revealed to be the direct binding of trivalent arsenic to cysteine thiols of PML-RARα, resulting in its conformational change, oligomerization, and enhanced SUMOylation/ubiquitination and degradation.[13,15] However, the success of ATO in APL treatment is hardly transferred into non-APL malignancies.[12]

Binding of trivalent arsenic to thiol groups of protein cysteine residues is regarded as the molecular mechanism explaining the biological effects of arsenic.[2,16] Due to the wide distribution of cysteine in cellular proteins,[17] the traditional arsenicals that lack a specific targeting group were found binding promiscuously to different proteins, leading to complicated cellular toxicity.[16,18−23] Furthermore, the reversible covalent nature of an arsenic−thiol bond constrains the K_d values of traditional arsenicals at the μM level,[24−26] resulting in a low potency of most arsenicals for inhibition of either protein activity or cancer cell proliferation.[16,27] In contrast, most of the approved drugs possess high selectivity and nM potency toward protein targets that are critical for

Received: November 6, 2023
Revised: March 20, 2024
Accepted: March 22, 2024
Published: April 1, 2024

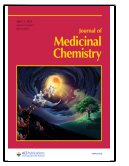

https://doi.org/10.1021/acs.jmedchem.3c02076
J. Med. Chem. 2024, 67, 5458−5472

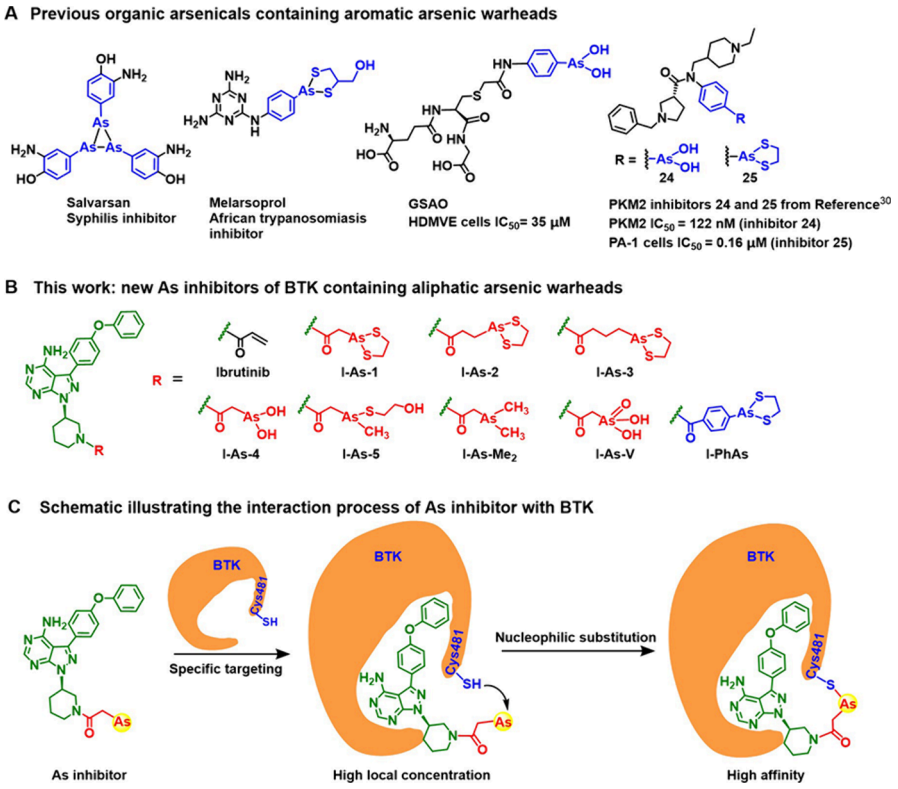

Figure 1. (A) Previous organic arsenicals containing the bulky and rigid aromatic arsenic warheads (blue). (B) Chemical structures of new As inhibitors of BTK containing flexible aliphatic arsenic warheads (red) and guiding group (green). (C) Schematic illustrating the interaction process of the As inhibitor with BTK. When the guiding group interacts selectively with the ATP binding pocket of BTK, it brings the As warhead in close proximity with Cys481, facilitating a high local concentration, which results in the formation of a covalent bond between the reactive arsenic warhead and thiol of Cys481. The biorthogonal nature of the guiding group and the reactive As warhead in the same molecule synergistically will enhance specific targeting and binding affinity of the As inhibitor toward targeted protein.

cancer survival.[28,29] The issue of low potency and toxic side effect as results of weak binding affinity and poor selectivity precludes most of the existing arsenicals from being promising candidates for non-APL cancer treatment.[12]

Phenylarsonous acid, an aromatic arsenical that had been used for the synthesis of melarsoprol[5] and GSAO,[7] was recently employed as a warhead for reversible covalent targeting pyruvate kinase M2 (PKM2), and the obtained phenylarsonous drug exerts efficacious inhibition of PKM2-dependent tumor growth (Figure 1A).[30] This work demonstrates the potential of arsenic as a reversible covalent warhead. However, due to its relatively large size and rigidity compared with the widely used acrylamide and chloroacetamide warheads, we wonder if phenylarsonous acid can be compatible with the existing covalent targeting inhibitors that have been validated for medical use.[31,32]

To answer this question, in this study, we aimed to find the proper aliphatic arsenic warheads (Figure 1B) whose molecular size and flexibility are similar to the acrylamide/chloroacetamide warheads.[31,32] We envision that the rational designed arsenic-based reversible covalent targeting inhibitor (As inhibitor) featuring the optimized aliphatic As warhead and the guiding group from the well-developed covalent targeting inhibitor could achieve desired affinity and selectivity that were not obtained by traditional arsenicals before. To this end, we chose Bruton's tyrosine kinase (BTK), a nonreceptor kinase that plays a crucial role in oncogenic signaling and survival of B-cell-related non-APL malignancies, as the model targeted protein to develop the new As inhibitors.[33,34] Among the several acrylamide-based covalent inhibitors that bind Cys481,[35,36] a noncatalytic cysteine proximal to the ATP binding pocket of BTK, ibrutinib,[35] is particularly noteworthy and has been approved by FDA as a breakthrough therapy for B-cell malignancies.[37−39] We therefore employed the kinase-recognition scaffold (green) of ibrutinib (Figure 1B) as the guiding group for the development of the new As inhibitors.

RESULTS AND DISCUSSION

Design of As Warheads and As Inhibitors. As shown in Figure 1B, we designed and synthesized a series of new As inhibitors that comprised the guiding group (green) and different As warheads (red). Specifically, (i) **I-As-1**, **2**, and **3** denote aliphatic As inhibitors containing one, two, and three methylene groups between the guiding group and trivalent arsenic warhead, which was complexed with an ethane-1, 2-dithiol (EDT) to prevent its oxidation[30,40]; (ii) **I-As-4**, an EDT-free counterpart of **I-As-1**, was designed to investigate the effect of thiol protection on As inhibitors' activity; (iii) to study the impact of methylation on the binding of As warhead with thiol, we further introduced one and two methyl groups to the trivalent As warhead of **I-As-4**, obtaining **I-As-5** and **I-As-Me$_2$**, respectively. **I-As-Me$_2$**, whose thiol binding sites were completely blocked by methyl groups, serves as a negative control to study the contribution of arsenic−thiol binding on inhibitors' activity; (iv) **I-As-V** (a pentavalent counterpart of **I-As-1**) was also designed as a negative control because the pentavalent arsenic was not expected to form arsenic−thiol bond with BTK; (v) **I-PhAs**, an aromatic As inhibitor with a

https://doi.org/10.1021/acs.jmedchem.3c02076
J. Med. Chem. 2024, 67, 5458−5472

phenylarsonous warhead, was designed to compare its activity with the aliphatic ones. When the guiding group interacts selectively with the ATP binding pocket of BTK, it brings As warheads in close proximity with Cys481, facilitating a high local concentration,[31,41] which results in the formation of covalent bond between the reactive arsenic warhead and thiol of Cys481 (Figure 1C). The biorthogonal nature of the guiding group and the reactive As warhead in the same molecule will synergistically enhance specific targeting and binding affinity of the As inhibitor toward targeted protein.

Synthesis of As Warheads and As Inhibitors. In general, aliphatic arsenic warheads were synthesized via the nucleophilic substitution reaction of alkaline arsenite with alkyl halides according to the synthesis route outlined in Scheme 2.[42−47] All the As warheads contained a carboxylic acid to facilitate the conjugation with the cyclic secondary amine of guiding group. **As-V** was directly obtained by the substitution reaction of arsenite with chloroacetic acid in alkaline solution (Scheme 1A).[42] Aromatic **PhAs** was obtained by a substitution reaction of an arsenate anion with aryl diazonium salt followed by reduction using EDT (Scheme 1A).[45] The organic arsenic intermediates, (3-hydroxypropyl)arsonic acid and (4-hydroxybutyl)arsonic acid of **As-2** and **As-3**, respectively, were prepared by substitution reactions of arsenite with 3-chloro-1-propanol and 1,4-dibromobutane.[43,44] The obtained organoarsenate intermediates were further oxidized to obtain carboxylated organoarsenate[48] followed by reduction with EDT to yield the **As-2** and **As-3** (Scheme 1A). Methylated As warheads, **As^{V}-5** and **As^{V}-Me$_2$**, were prepared by first synthesizing methylarsenic dibromide and dethylarsenic bromide,[46] respectively, followed by substitution with chloroacetic acid to obtain the desired products (Scheme 1B).

Scheme 1. Synthesis Route of (A) Arsenic Warheads As-V, As-2, As-3, and PhAs and (B) Methylated Arsenic Warheads As^{V}-5 and As^{V}-Me$_2$[a]

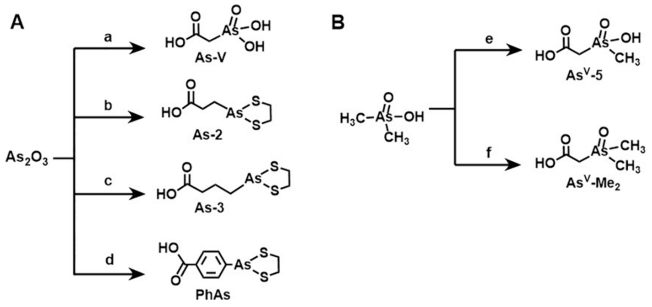

[a]Reagents and conditions: (a) chloroacetic acid, NaOH, rt; then acetic acid, $BaCl_2{\cdot}2H_2O$, rt; then Amberlite IR-120 (H^+), 81%; (b) 3-chloro-1-propanol, NaOH, 50 °C; then $NaIO_4$, $RuCl_3$, rt; then EDT, rt, 35%; (c) 1,4-dibromobutane, NaOH, 80 °C; then $NaIO_4$, $RuCl_3$, rt; then EDT, rt, 37%; (d) Na_2CO_3, $CuSO_4{\cdot}5H_2O$, 80 °C; then 4-aminobenzoic acid, $NaNO_2$, HCl, 0 °C to rt; then EDT, rt, 39%; (e) HBr, 130 °C; then chloroacetic acid, NaOH, rt; (f) HBr, rt; then chloroacetic acid, NaOH, rt.

The obtained carbonylated As warheads were subsequently activated by EDC/NHS and further conjugated to the cyclic secondary amine of the guiding group, obtaining **I-As-2**, **3**, **V**, and **I-PhAs** (Scheme 2). **I-As-1** was obtained through reduction of **I-As-V** and complex with EDT. **I-As-4** was obtained by reduction with GSH. **I-As-5** and **I-As-Me$_2$** were obtained via reduction of **I-As^{V}-5** and **I-As^{V}-Me$_2$** and complex with mercaptoethanol. Detailed synthesis procedures are described in the Experimental Section and SI, and each inhibitor was well characterized by HPLC-ESIMS and NMR (Figures S1−12).

Inhibitory Potency and In Situ Reactivity of As Inhibitors. To evaluate the inhibitory potency of the new As inhibitors, we measured their IC_{50} values toward recombinant BTK (Figure 2A). Our results showed an IC_{50} of 0.91 nM for ibrutinib, consistent with the result reported in the literature.[35,49] The aliphatic **I-As-1**, **2**, **3**, **4**, and **5** were found to retain the inhibitory potency against BTK, with IC_{50} values in the range from 2.35 to 3.56 nM. The IC_{50} values of **I-As-1**, **2**, and **3** gradually increase, indicating that the flexible spacer lengths within three methylene groups had a slight influence on the potency of As inhibitors (Figure 2A). The small difference between the IC_{50} values of EDT-protected **I-As-1** (IC_{50}, 2.35 nM) and EDT-free **I-As-4** (IC_{50}, 3.56 nM) indicated that the introduction of EDT has a minor impact on the activity of As inhibitors. The potency of **I-As-5** (IC_{50}, 2.79 nM) on BTK is comparable to those of **I-As-1** and **I-As-4**, suggesting that the arsenic warhead, whether it possesses one or two thiol binding sites, has a similar inhibitory activity. The low potency of both negative control inhibitors, **I-As-Me$_2$** (IC_{50}, 28.02 nM) and pentavalent **I-As-V** (IC_{50}, 13.85 nM), as well as the nontargeted arsenicals (**As-2**, **As-3**, **PhAs**, **iAs^{III}**, **MMA^{III}**, **DMA^{III}**, and **As-V**, IC_{50} were not obtained) demonstrate that both the reactive trivalent arsenic warhead and the guiding group are essentially important for high affinity binding of As inhibitors to BTK (Figure 2A). **I-PhAs** (IC_{50}, 479.3 nM) showed a weak inhibitory activity (Figure 2A), indicating that the phenylarsenate warhead was not well compatible with the guiding group toward BTK inhibition.

We further investigated the in situ reactivity of As inhibitors in live Ramos Burkitt's lymphoma cells that endogenously express BTK. PCI-33380 (Figure S13), a Bodipy-FL fluorophore-modified ibrutinib derivative, was applied to detect the competitive binding of inhibitors to BTK.[49] As shown in Figure 2B, PCI-33380 formed a stable adduct with BTK in live Ramos cells after 1 h incubation. Pretreatment of cells with 10 nM ibrutinib completely eliminated the PCI-33380-labeled BTK band, indicating its high potency. Meanwhile, pretreatment of cells with 1×10^4 nM **I-As-Me$_2$**, **I-As-V**, guiding group alone, or nontargeted arsenicals had no influence on the fluorescence of BTK (Figure 2B and Figure S13), suggesting their low binding activity to BTK. We observed a concentration-dependent competitive binding of **I-As-1** to BTK, and 60 nM **I-As-1** was observed to effectively occupy intracellular BTK, much more potent than either the guiding group or As warhead alone (Figure 2B and Figure S13). As shown in Figure S13, **I-As-2**, **3**, **4**, and **5** also efficiently bind to BTK at 60−200 nM. The spacer length within three methylene groups showed a minor influence on the cellular activity of As inhibitors. In addition, the comparison between **I-As-1**, **4**, and **5** revealed that either EDT protection or one or two thiol binding sites of As warheads slightly impact the efficacy of As inhibitors. We found that **I-PhAs** was not able to occupy BTK even when its concentration reached 1×10^4 nM (Figure 2B). Together with the enzyme inhibitory results (Figure 2A), we demonstrated that the bulky and rigid phenylarsonous warhead was not compatible with the guiding group of ibrutinib, an elegant inhibitor match perfectly with the ATP binding pocket of BTK.

https://doi.org/10.1021/acs.jmedchem.3c02076
J. Med. Chem. 2024, 67, 5458−5472

Scheme 2. Synthesis Route of As Inhibitors I-As-1, I-As-2, I-As-3, I-As-4, I-As-5, I-As-Me$_2$, I-As-V, and I-PhAs[a]

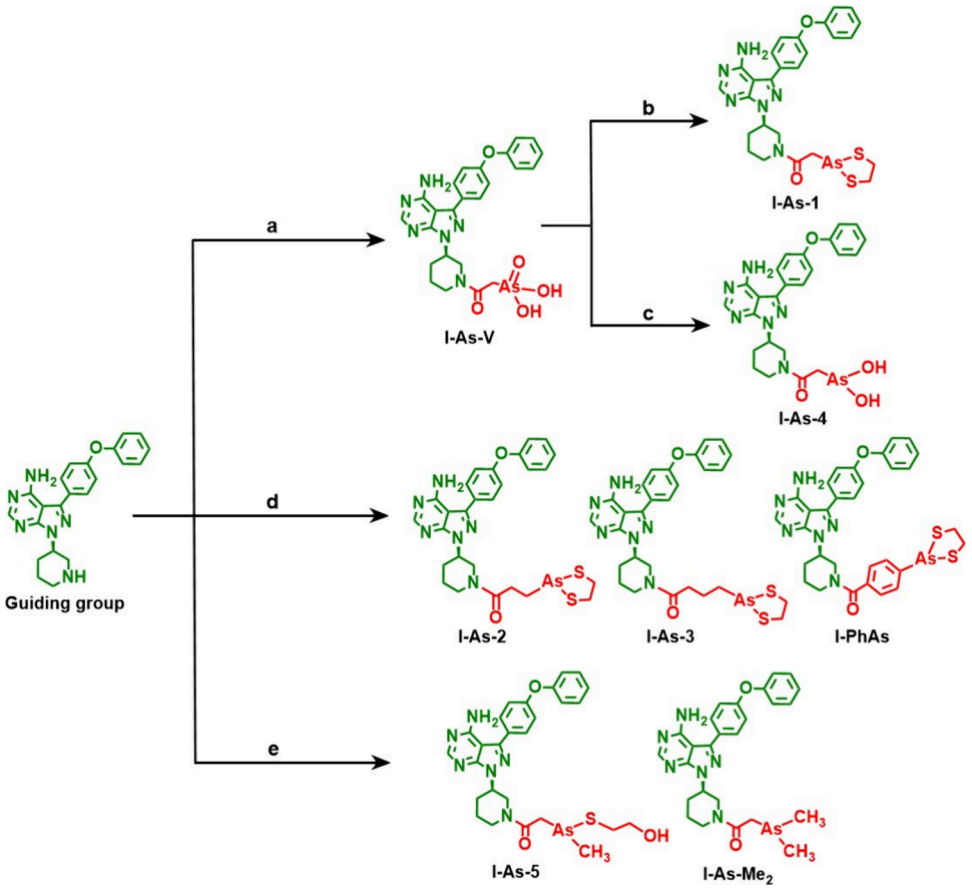

[a]Reagents and conditions: (a) **As-V**, EDCI, NHS, TEA, rt, 60%; (b) EDT, rt, 78%; (c) GSH, rt, 21%; (d) **As-2**, **As-3**, or **PhAs**, EDCI, NHS, TEA, rt, 59% for **I-As-2**, 56% for **I-As-3**, and 65% for **I-PhAs**; (e) As^{V}**-5** or As^{V}**-Me$_2$**, EDCI, NHS, TEA, rt; then mercaptoethanol, rt, 19% for **I-As-5** and 16% for **I-As-Me$_2$**.

Molecular Docking. We further applied molecular docking analysis to study the interactions between As inhibitors and BTK. The key direct interactive residues, Thr474, Glu475, Cys481, and Phe540, were shown in the BTK-ibrutinib cocrystal structure (PDB ID: 5P9J).[50] The docking results demonstrate that both **I-As-1** and ibrutinib form hydrogen bonds with Thr474 and Glu475 and a hydrophobic interaction with Phe540 (Figure 3A), featuring a similar posture and interactive model inside the ATP binding pocket of BTK. Similar results were also obtained in the docking analysis of **I-As-2**, **3**, **4**, and **5** (Figure S14), demonstrating that the small and flexible aliphatic As warheads were well compatible with the guiding group in the ATP binding pocket of BTK. The binding energies of As inhibitors with different arsenic warheads were as low as −10 kcal/mol (Table S1), indicating that the interactions between aliphatic As inhibitors and BTK were stable. The molecular docking result of **I-PhAs** showed that the guiding group of **I-PhAs** interacted with the ATP-binding domain of BTK in a way similar to ibrutinib. However, the bulky and rigid phenylarsonous warhead of **I-PhAs** is far away (10 Å) from the thiol group of Cys481, precluding the formation of a covalent As−thiol bond between **I-PhAs** and BTK (Figure 3B). The molecular docking results were consistent with the results of enzyme inhibitory (Figure 2A) and in situ reactivity (Figure 2B) of As inhibitors. We therefore chose aliphatic As inhibitors for the following study.

As Inhibitors' Effect on the BTK-Mediated BCR Signaling Pathway. Having demonstrated the potency of As inhibitors, we further investigated their activity against the BTK-mediated BCR signaling pathways in live cells through SDS-PAGE immunoblotting. As shown in Figure 4A, anti-IgM, a mimic of BCR-antigen, was used to stimulate Ramos cells and activate the BCR signaling pathway, resulting in phosphorylation of BTK and its upstream (Syk) and downstream (PLCγ2, Erk1/2) kinases.[51] As shown in Figure 4B and Figure S15, reactive As inhibitors exhibited comparable activities to inhibit the phosphorylation of BTK as well as its downstream kinase substrates (PLCγ2, Erk1/2) in a concentration-dependent manner. The incomplete suppression of pErk1/2 by ibrutinib and **I-As-1** was also observed in other studies,[52,53] the reason for which is some compensatory effectors besides BTK could also activate the phosphorylation of Erk1/2,[54] resulting in incomplete suppression of p-ERK1/2 by ibrutinib and As inhibitors. Effective inhibition of BTK phosphorylation was observed when 64 nM reactive trivalent As inhibitors were applied, while **I-As-Me$_2$**, **I-As-V**, guiding group alone and nontargeted arsenicals had no effect on BCR signaling even when its concentration reached 1000 nM. Phosphorylation of the upstream Syk was not affected, indicating the high in situ selectivity of As inhibitors toward BTK (Figure 4B and Figure S15).

Antiproliferative Activities and Cell Uptake of As Inhibitors. The antiproliferative activities of As inhibitors

https://doi.org/10.1021/acs.jmedchem.3c02076
J. Med. Chem. 2024, 67, 5458−5472

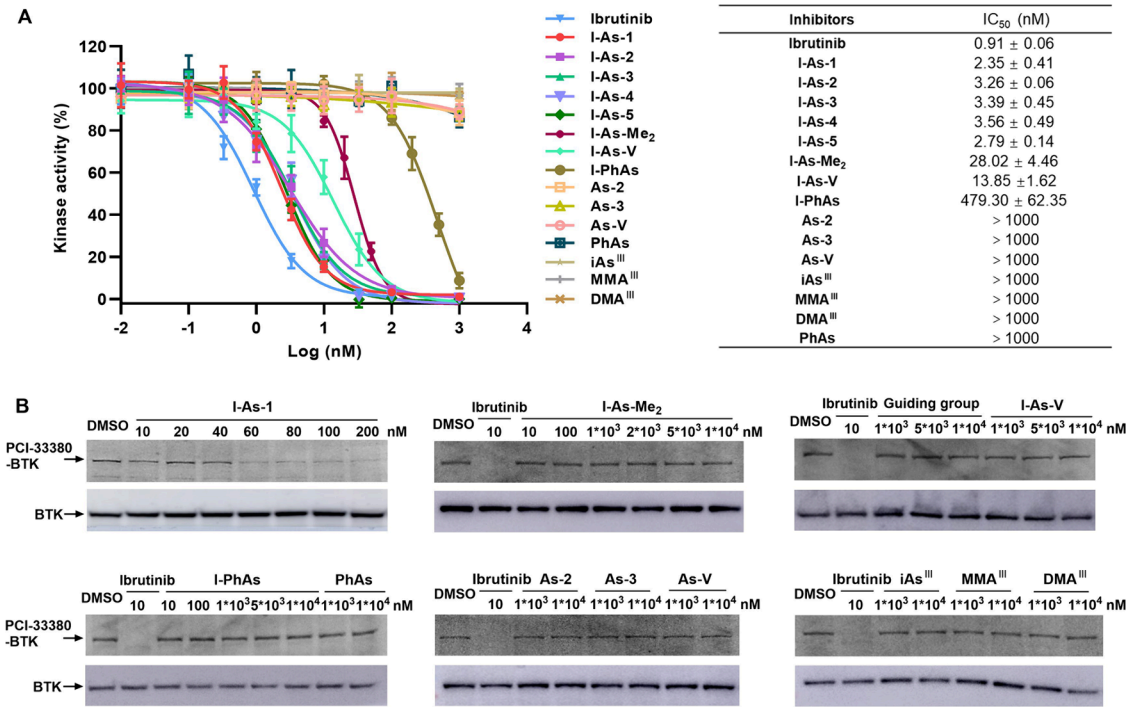

Inhibitors	IC_{50} (nM)
Ibrutinib	0.91 ± 0.06
I-As-1	2.35 ± 0.41
I-As-2	3.26 ± 0.06
I-As-3	3.39 ± 0.45
I-As-4	3.56 ± 0.49
I-As-5	2.79 ± 0.14
I-As-Me_2	28.02 ± 4.46
I-As-V	13.85 ±1.62
I-PhAs	479.30 ± 62.35
As-2	> 1000
As-3	> 1000
As-V	> 1000
iAs^{III}	> 1000
MMA^{III}	> 1000
DMA^{III}	> 1000
PhAs	> 1000

Figure 2. *In vitro* and cellular evaluation of the potency of As inhibitors toward BTK. (A) Dose−response curves of the activity of recombinant BTK treated with different inhibitors. IC_{50} values were obtained by fitting the dose−response curves of BTK activity as a function of inhibitors' concentration. (B) In situ profiling the concentration-dependent binding between inhibitors and cellular BTK by competitive fluorescence labeling in live Ramos Burkitt's lymphoma cells. Arrows indicate that the predominant band labeled by PCI-33380 was BTK as confirmed by SDS-PAGE immunoblotting (lower).

against Ramos cells were investigated through a cell viability assay (Figure 5A and Table S2). As expected, the IC_{50} values of **I-As-1**, **2**, and **3** are 0.52, 1.01, and 1.29 μM, respectively. This trend aligns well with their inhibition activity toward BTK (Figure 2A). The IC_{50} of **I-As-Me$_2$** was determined to be 52.61 μM, and the IC_{50} of pentavalent **I-As-V** was not obtained in the concentration range tested. We found that the reactive As inhibitors exhibited significant higher antiproliferative activities than both of ibrutinib (IC_{50}, 12.03 μM) and nontargeted trivalent arsenicals (IC_{50}, 3.66−7.89 μM) (Table S2). To explain the possible cause of this observation, we determined the cellular uptake of As inhibitors and ibrutinib.

Noteworthily, the arsenic atom in As inhibitors can serve as an idea element tag for cellular uptake analysis through using inductively coupled plasma mass spectrometry (ICPMS), a powerful element quantification tool.[55−57] For ibrutinib that lacks an arsenic atom, HPLC-ESIMS was applied to determine its concentration. As shown in Figure 5B, high uptake of nontargeted arsenicals was observed. Due to the lack of guiding group, their cytotoxicity showed no significant difference between Ramos and HepG2 cells that do not express BTK (Figure 5C and Table S2). In contrast, the cytotoxicity of As inhibitors is higher in Ramos cells than that in HepG2 cells (BTK negative), suggesting BTK as the specific target of As inhibitors. We found a higher uptake of trivalent As inhibitors compared to that of ibrutinib, which could be due to their higher hydrophobicity, as confirmed by measuring their retention time in RPLC (Figure S16). Specifically, the uptake of **I-As-1** was 3.4- to 13.8-fold higher than that of ibrutinib (Figure 5B) at the incubation concentration from 1 to 20 μM, which partially explains the higher (23.1-fold) antiproliferative activity of **I-As-1** compared to ibrutinib. The uptake of **I-As-1** was about 2.0-fold higher than that of **I-As-Me$_2$**, which contains an unreactive arsenic warhead. However, the cytotoxicity of **I-As-1** (IC_{50}, 0.52 uM) was about 2 orders of magnitude higher than that of **I-As-Me$_2$** (IC_{50}, 52.61 uM), indicating that the high activity of As inhibitors is due to not only their higher cellular uptake but also the binding between the As warhead and Cys481 of BTK.

Reversible Covalent Nature of As Inhibitors. We further attempted to explain the high activity of As inhibitors by exploring whether As inhibitors form reversible covalent adducts with BTK. Reversible covalent inhibitors potentially have higher efficacy because they can be released from the protein−inhibitor adduct when the target proteins degrade or loss the affinity toward inhibitors due to conformation change.[58−61]

To explore whether As inhibitors form reversible covalent adducts with BTK, we conducted a HPLC-ESIMS-based peptide mapping experiment to trace the binding of As inhibitors with tryptic peptide 467−487 that contains the targeted Cys481 residue (Figures S17 and S18). As expected, when ibrutinib-labeled BTK was treated with trypsin digestion procedures, i.e., protein reduction, IAA alkylation, and digestion, ibrutinib (irreversible) was found to form a stable adduct with peptide 467−487 (Figure S18A), and the signal of carbamidomethyl (CAM)-peptide alkylated by IAA was very low (Figure S18B). In contrast, no As inhibitor−peptide adduct was detected in the tryptic product of As inhibitor-labeled BTK, while the signal of CAM-peptide 467−487 was the same as that of BTK that was not incubated with any inhibitor (Figure S18C,D). This result indicated that the As inhibitor dissociated from BTK upon the disruption of the protein structure, demonstrating the reversible covalent nature

https://doi.org/10.1021/acs.jmedchem.3c02076
J. Med. Chem. 2024, 67, 5458−5472

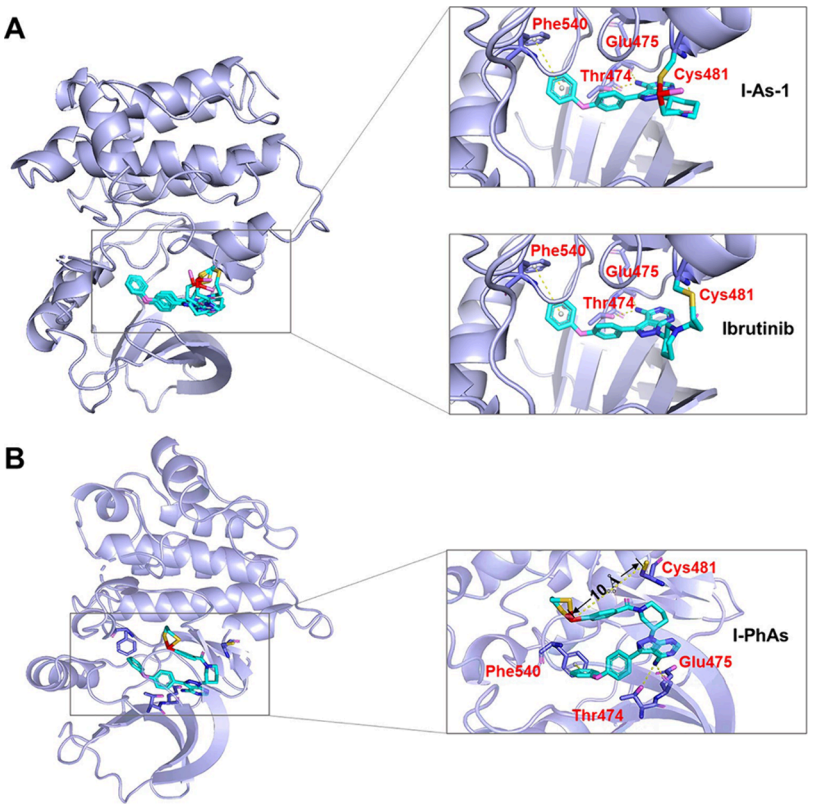

Figure 3. Binding mode comparison of **I-As-1**, **I-PhAs**, and ibrutinib with BTK (PDB ID: 5P9J). Sulfur and As atoms are indicated as yellow and red, respectively. (A) Both **I-As-1** and ibrutinib formed a hydrogen bond with Thr474 and Glu475 and a hydrophobic interaction with Phe540, featuring a similar pose in the ATP binding pocket of BTK, which demonstrated that the small and flexible aliphatic As warheads were well compatible with the guiding group in the ATP binding pocket of BTK. (B) Guiding group of **I-PhAs** formed a hydrogen bond with Thr474 and Glu475 and a hydrophobic interaction with Phe540. However, the bulky and rigid phenylarsonous warhead of **I-PhAs** is far away (10 Å) from the thiol of Cys481, precluding the formation of a covalent As−thiol bond between the As warhead and BTK.

of the arsenic−thiol bond. To evaluate the binding strength (reversibility) between As inhibitors and BTK, we conducted a competitive (As inhibitors VS ibrutinib) binding experiment. Specifically, when BTK was preincubated with As inhibitors followed by the addition of ibrutinib, the competitive binding of As inhibitors to BTK resulted in a lower ibrutinib−peptide adduct (higher CAM-peptide 467−487 signal) and vice versa. The inhibitor-bound BTK % was calculated by normalizing the signal of CAM-peptide 467−487 with internal standard peptide 219−236, whose signal was stable and at the same level as CAM-peptide. We found the BTK % of **I-As-1**, **2**, and **3** slightly reduced, indicating that with the increase in spacer length, the inhibitors' affinity toward Cys481 slightly decreased (Figure 5D). The evaluated reversibility of **I-As-4** and **I-As-5** was also found to agree with their BTK and Ramos cells IC_{50} values and the in situ reactivity, indicating that the higher potency of **I-As-1** came from its higher binding affinity to BTK (Figure 2A, Figure 5A,D, and Figure S13). **I-As-Me$_2$**, **I-As-V**, guiding group alone, or nontargeted arsenicals were not found to form a stable complex with BTK (Figure 5D).

The reversible covalent nature of As inhibitors was further demonstrated through a cellular washout experiment.[58] As shown in Figure 5E and Figure S19, **I-As-1** gradually dissociated from BTK with prolonged residence time, showing 21% BTK occupancy 20 h after washout, and the fluorescence of BTK recovered by 79% (Figure 5E). A minor fluorescence of BTK observed in the ibrutinib-treated cells was due to the labeling of PCI-33380 to newly synthesized BTK.[58] **I-As-Me$_2$**, which contains an unreactive arsenic warhead, is unable to block the binding of PCI-33380 to BTK. These findings support the reversible covalent nature of As inhibitors and further explain their high activity.

Selectivity of As Inhibitors. Relying on the reversible covalent nature of the arsenic−thiol bond, the As inhibitors were expected to achieve high selectivity as a benefit of avoiding the formation of permanent stable adducts with off-target proteins.[58−61] To evaluate the selectivity of As inhibitors in Ramos cells, we conducted a concentration-dependent competition labeling experiment using a high concentration of PCI-33380 (20 μM) to trace their nonspecific binding with off-target proteins (Figure S20A).[49,60] We observed a concentration-dependent competition manner of **I-As-1** or ibrutinib for BTK (Figure S20B,C). Meanwhile, for the off-target proteins, their fluorescence was not fully competed by **I-As-1** even when its concentration reached 20 μM, verifying As inhibitor's higher specificity to targeted kinase compared with off-target proteins. However, further efforts could still be made to specifically test the kinome selectivity of As inhibitors for BTK compared to other kinases.[58]

***In Vivo* Antitumor and Pharmacokinetic Studies.** The high antiproliferative potency of As inhibitors drove us to study the *in vivo* treatment of SCID mice carrying cancer cells-xenograft tumor. We did not choose Ramos cells because forming suitable xenograft tumor for *in vivo* experiments is difficult. OCI-LY10, a cell line of activated B-cell-like diffuse large B-cell lymphoma, is more prone to form mouse xenograft

https://doi.org/10.1021/acs.jmedchem.3c02076
J. Med. Chem. 2024, 67, 5458−5472

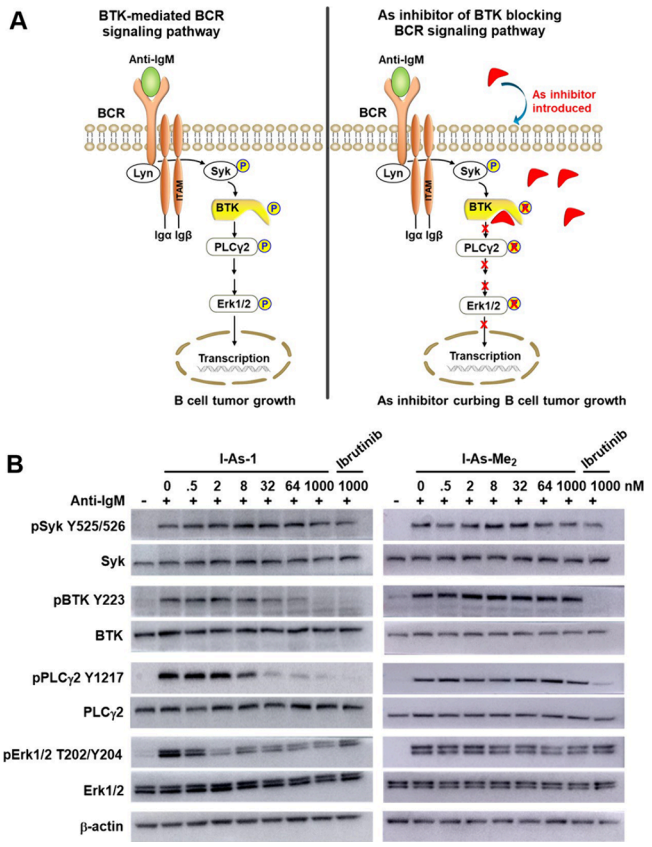

Figure 4. Inhibition of BCR signaling by As inhibitors. (A) Schematic illustrating the BTK-mediated BCR signaling pathway and its inhibition by As inhibitors. (B) Concentration-dependent inhibition of BCR stimulation-induced phosphorylation in Ramos cells by As inhibitors as determined by SDS-PAGE immunoblotting. Blots were probed with the indicated antibodies to detect the phosphorylation of kinases along the BCR signaling pathway.

tumors with an initial volume of approximately 100 mm^3 for *in vivo* experiments (Figure 6B).[62] Compared with Ramos cells, As inhibitors and ibrutinib were found to exhibit a higher cytotoxicity (Figure 6A) and a more efficient blocking of the BCR signaling pathway (Figure S21) in OCI-LY10 cells. **I-As-1**, the most potent one, was chosen as the representative to study the antitumor activity of As inhibitors. As shown in Figure 6B,C, the average tumor size after treatment with 20 μmol/kg ibrutinib was reduced by 41% compared to the vehicle group at the end of *in vivo* experiments. In contrast, the 20 μmol/kg nontargeted arsenical group showed negligible inhibition of tumor growth. Encouragingly, tumor sizes were reduced by 66% in the 20 μmol/kg **I-As-1** group, showing a significant antitumor activity. Moreover, after 14 days of treatment, the mice in **I-As-1** group slightly gained weight (Figure 6D) and no poisoning symptom was observed, indicating that **I-As-1** was well-tolerated by SCID mice. At the end of treatment, mice were sacrificed and the *in vivo* distribution of As inhibitors was studied (Figure S22). The obtained results showed a high content of arsenic in tumor issue. However, **I-As-1** was also found present in the lung, liver, and kidney, implying further efforts could be made to improve As inhibitors' tumor accumulation.[63]

We further revaluated the pharmacokinetic profiles of **I-As-1** and ibrutinib in mice after intravenous injection at a dose of 20 μmol/kg. The obtained results showed that **I-As-1** exhibited a half-life of 0.607 h, longer than that of ibrutinib (0.277 h) (Figure S23). Moreover, we conducted a size exclusion chromatography (SEC)-ICPMS experiment to track the state of **I-As-1** in mice plasma. We found that most of the As inhibitor was bound to plasma proteins, and only a small portion was in its free state. With the addition of EDT, the As inhibitor was replaced by EDT and released from plasma proteins (Figure S24), indicating that the reversible covalent As−thiol bond was responsible for the binding of the As inhibitor to plasma proteins. Reversible covalent binding of the As inhibitor to plasma proteins prolongs the retention time of the As inhibitor in mice blood. As inhibitors could gradually dissociate from plasma proteins to achieve a longer lasting efficacy, which could be another reason explaining the high *in vivo* potency of As inhibitors.

CONCLUSIONS

In summary, we have established aliphatic trivalent arsenicals as new types of reversible covalent warheads for targeted protein inhibition. We found that conjugating the bulky and rigid phenylarsonous warhead with the well optimized guiding group of ibrutinib compromised the binding activity toward targeted kinase. In contrast, the small and flexible aliphatic As warheads were well compatible with the guiding group of ibrutinib for BTK binding. Through *in vitro* and cellular studies, we proved that the aliphatic As inhibitor's high affinity and selectivity came from the synergetic binding of guiding group and As warhead to the targeted kinase. The effects of aliphatic As warheads' valency, thiol protection and methylation state, as well as spacer length on As inhibitors' activity were studied. The developed As inhibitors achieved an nM inhibitory potency toward BTK and the oncogenic BCR signaling pathway that was not realized by traditional arsenicals before. On the basis of the promising targeting strategy developed in this study, new arsenic-based reversible covalent inhibitors could be created by conjugating aliphatic As warheads with the optimized guiding groups.[31,32] The effective treatment of different non-APL malignancies by new arsenic drugs will greatly expand the medicinal value of arsenic.

EXPERIMENTAL SECTION

General Information and Methods. All chemicals used in this study were of analytical grade or better without further purification. Arsenic trioxide (As_2O_3), chloroacetic acid, trifluoroacetic acid (TFA, HPLC grade), and acetonitrile (ACN, HPLC grade) were purchased from Sigma-Aldrich (USA). 3-Chloro-1-propanol, 1,4-dibromobutane, ruthenium chloride ($RuCl_3$), sodium periodate ($NaIO_4$), barium chloride dihydrate ($BaCl_2{\cdot}2H_2O$), sodium nitrite ($NaNO_2$), 4-aminobenzoic acid, 1-ethyl-3-(3-dimethyllaminopropyl)carbodiimide hydrochloride (EDCI), *N*-hydroxysuccinimide (NHS), 1-hydroxybenzotriazole(HOBT), triethylamine (TEA), kinase-recognition scaffold (guiding group, 3-(4-phenoxyphenyl)-1-(piperidin-3-yl)-1*H*-pyrazolo[3,4-*d*]pyrimidin-4-amine, BTK inhibitor 1R enantiomer), 1,2-ethanedithiol (EDT), iodoacetamide (IAA), and mercaptoethanol were purchased from Aladdin (China). Ibrutinib and **iAs^{III}** (sodium arsenite) were purchased from Innochem (China). **MMA^{III}** and **DMA^{III}** were prepared following the procedures reported in the literature.[64]

For purification of the synthesized compounds, a preparative HPLC system (LC-16P, Shimadzu, Kyoto, Japan) equipped with a Shimadzu SPD-16 UV detector, 5 mL sampling loop, and a Shimadzu C18-ST column (10.0 I.D. × 250 mm in length, 5 μm particle size) was used. Chromatographic analysis was carried out on an LC-20AD analytical HPLC system (Shimadzu, Japan) using an Inertsil ODS-3 C18 column (4.6 I.D. × 150 mm in length, 5 μm particle size). HPLC

https://doi.org/10.1021/acs.jmedchem.3c02076
J. Med. Chem. 2024, 67, 5458−5472

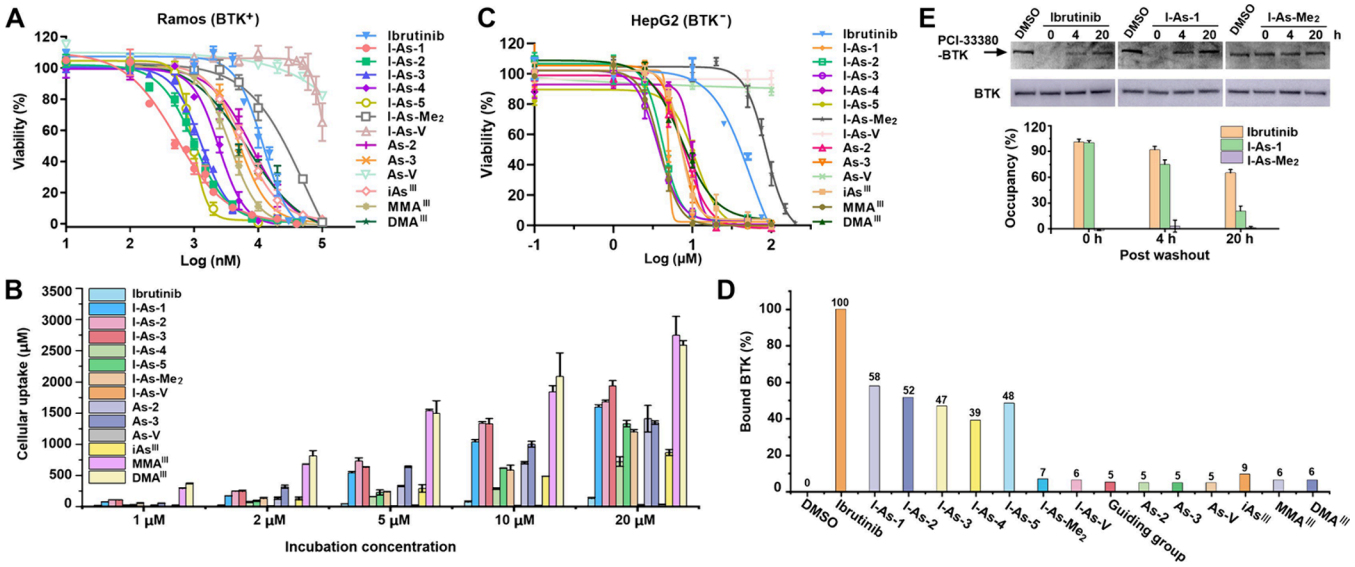

Figure 5. Cellular study of the efficacy of As inhibitors and ibrutinib. (A) Dose−response curves of the viability of Ramos cells (BTK$^+$) treated with different inhibitors. (B) Concentration-dependent uptake of inhibitors by Ramos cells. (C) Dose−response curves of the viability of HepG2 cells (BTK$^-$) treated with different inhibitors. Data represent average values ± s.e. for triplicate measurements from two independent experiments. Evaluation of the reversible covalent nature of As inhibitors toward BTK. (D) Normalized percentage of inhibitor-bound BTK by tracing the binding of inhibitors with tryptic peptide 467−487. (E) Cellular washout experiment evaluating the binding of ibrutinib, **I-As-1**, and **I-As-Me$_2$** with cellular BTK in Ramos cells. Arrows indicate that the predominant band labeled by PCI-33380 was BTK as confirmed by SDS-PAGE immunoblotting (lower).

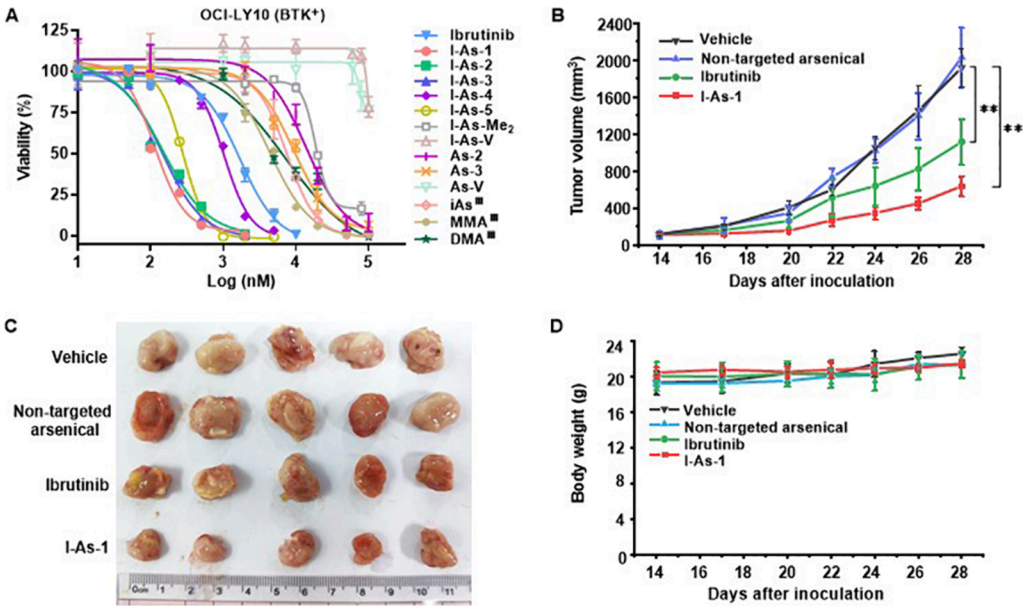

Figure 6. Cellular and *in vivo* study of the efficacy of As inhibitors. (A) Dose−response curves of the viability of OCI-LY10 cells (BTK$^+$) treated with different inhibitors. (B) Mean volume of xenograft tumor in SCID mice treated with vehicle, nontargeted arsenical, ibrutinib, and **I-As-1**. SCID mice were injected subcutaneously with OCI-LY10 cells. When xenograft tumors' volume reached approximately 100 mm^3, mice were randomized into four groups (n = 5/group) and treated with **I-As-1**, ibrutinib, nontargeted arsenical, or vehicle once a day for 14 days. Inhibitors (20 μmol/kg) were administered via the tail vein as a clear solution in an optimized vehicle (87.5% saline, 10% Solutol HS 15, 2.5% DMSO). $^{**}P <$ 0.01 indicates statistical significance of tumor growth inhibition. (C) Photographs of tumors excised from the mice treated with vehicle, nontargeted arsenical, ibrutinib, or **I-As-1** for 14 days. (D) The mice body weights changed over time.

analyses confirmed that all As inhibitors exhibit purity greater than 95%. A Bruker Impact II electrospray ionization quadrupole time-of-flight mass spectrometer (ESI-Q-TOF-MS) (Germany) was used for characterizing the reaction intermediates and final products. ^{1}H NMR and ^{13}C NMR spectra were recorded on a Bruker Advance 500 (^{1}H, 500 MHz; ^{13}C, 125 MHz) spectrometer at ambient temperature. A quadrupole-based inductively coupled plasma mass spectrometer (ICPMS) (NEXION 2000, PerkinElmer, SCIEX, Canada) was used for quantification of arsenic. A NEXION 2000 ICPMS (PerkinElmer, SCIEX, Canada) coupled with size exclusion chromatography (SEC, Waters Xbridge Protein BEH 4.6 I.D. × 300 mm in length, 2.5 μm particle size) was used for analyzing the binding of the arsenic inhibitor to plasma proteins using a mobile phase of 100 mM ammonium acetate at a flow rate of 0.3 mL/min.

Synthesis of Arsonoacetic Acid (As-V). Following the method described by Nancekivell et al.,[42] arsenic trioxide (1.2 g, 6 mmol) and

https://doi.org/10.1021/acs.jmedchem.3c02076
J. Med. Chem. 2024, 67, 5458−5472

sodium hydroxide (1.44 g, 36 mmol) were dissolved in H_2O (12 mL) followed by addition of chloroacetic acid (570 mg, 6 mmol). The reaction mixture was stirred at room temperature for 4 h. The solution was then acidified with 2 mL of glacial acetic acid and cooled. Most of the remaining arsenic trioxide precipitate was filtered off. The filtrate was poured into a hot solution of $BaCl_2 \cdot 2H_2O$ (2.16 g, 8.8 mmol) in H_2O (6 mL) and stirred for 1 h. Barium arsonoacetate was filtered by suction after the solution was allowed to stand overnight and washed thoroughly with water. Barium arsonoacetate was stirred for 1 h with a sulfonated polystyrene resin (Amberlite IR-120, 2 mL wet volume) in its H^+ form. The resin was removed by filtration, and the filtrate was evaporated in vacuo to yield **As-V** (0.9 g, 81%) as a white solid.^{1}H NMR (500 MHz, D_2O): δ 3.62 (s, 2H). ^{13}C NMR (125 MHz, D_2O): δ 167.42, 38.29. HRMS (ESI): m/z Calcd for $C_2H_5AsO_5$ $[M + H]^+$, 184.9426, found 184.9440 (Figure S1).

*Synthesis of 3-(1,3,2-Dithiarsolan-2-yl)propanoic acid (**As-2**).* Arsenic trioxide (1.4 g, 7 mmol) and sodium hydroxide (1.7 g, 42 mmol) were dissolved in H_2O (12 mL), and 3-chloro-1-propanol (0.73 g, 7.7 mmol) was added dropwise with stirring at about 50 °C for 4 h. The solution was diluted with water to 20 mL and acidified with conc. HCl to pH 2. Subsequently, the reaction mixture was concentrated in vacuo and extracted twice with 45 mL of ethanol to eliminate most of the NaCl formed. The ethanol solution was evaporated to dryness, and the crude product was dissolved in water and stirred for 1 h with a sulfonated polystyrene resin (Amberlite IR-120, 2 mL wet volume) in its H^+ form. The pH was adjusted to 10.5 with LiOH and the solution evaporated to a small volume. The dilithium (3-hydroxypropyl)arsonate crystallized upon the addition of acetone.[43] A round-bottom flask was added with dilithium (3-hydroxypropyl)arsonate, sodium periodate (6.13 g, 8.7 mmol), $RuCl_3$ (33.6 mg), ACN (14 mL), H_2O (21 mL), and ethyl acetate (14 mL). The reaction mixture was stirred at room temperature for 12 h and then was washed with 40 mL of ethyl acetate. The aqueous layer was collected and acidized by conc. HCl to pH 2. Subsequently, the aqueous layer was then concentrated in vacuo and extracted twice with 100 mL of ethanol to eliminate most of the inorganic salt.[48] The above filtrate was stirred with EDT (5.26 g, 56 mmol) for 2 h at room temperature and finally purified by HPLC (a gradient elution was performed: starting from 95/5 H_2O/ACN to 10/90 H_2O/ACN in 25 min, 0.1% TFA, 5.0 mL/min) to yield **As-2** (0.65 g, 35%) as a white solid. ^{1}H NMR (500 MHz, $CDCl_3$): δ 3.39−3.31 (m, 4H), 2.67 (t, J = 7.6 Hz, 2H), 2.03 (t, J = 7.6 Hz, 2H). ^{13}C NMR (125 MHz, $CDCl_3$): δ 179.19, 41.88, 30.36, 30.34. HRMS (ESI) m/z: calcd. for C5H9AsO2S2 $[M + H]^+$, 240.9333, found 240.9335 (Figure S2).

*Synthesis of 4-(1,3,2-Dithiarsolan-2-yl)butanoic acid (**As-3**).* Arsenic trioxide (0.2 g, 1 mmol) and sodium hydroxide (0.24 g, 6 mmol) were dissolved in H_2O (3 mL), and then, 1,4-dibromobutane (1.08 g, 5 mmol) in 1 mL of ethanol was added dropwise with stirring at room temperature for 4 h. The reaction mixture was further refluxed at 80 °C for 12 h. Volatile organic residues were removed by vacuum distillation, and the residual solution was adjusted to pH 9 with conc. HCl. The remaining arsenic trioxide precipitate was filtered off. The filtrate was evaporated in vacuo to get the crude intermediate as a white solid.[44] A round-bottom flask was added with a crude intermediate, sodium periodate (0.43 g, 2.1 mmoL), $RuCl_3$ (2.4 mg), ACN (1.4 mL), H_2O (2.1 mL), and ethyl acetate (1.4 mL). The reaction mixture was stirred at room temperature for 12 h and then washed with 5 mL of ethyl acetate. The aqueous layer was collected and acidized by conc. HCl to pH 2. Subsequently, the reaction mixture was concentrated in vacuo and extracted twice with 10 mL of ethanol to eliminate most of the inorganic salt formed. The above filtrate was stirred with EDT (0.38g, 4 mmol) at room temperature for 2 h and finally purified by HPLC (a gradient elution was performed: starting from 95/5 H_2O/ACN to 10/90 H_2O/ACN in 25 min, 0.1% TFA, 5.0 mL/min) to yield **As-3** (95 mg, 37%) as a white solid. ^{1}H NMR (500 MHz, $CDCl_3$): δ 3.36−3.30 (m, 4H), 2.45 (t, J = 6.9 Hz, 2H), 1.90−1.81 (m, 4H). ^{13}C NMR (125 MHz, $CDCl_3$): δ 178.88, 41.75, 35.96, 35.01, 21.11. HRMS (ESI): m/z Calcd for $C_6H_{11}AsO_2S_2$ $[M + H]^+$, 254.9489, found 254.9504 (Figure S3).

*Synthesis of 4-(1,3,2-Dithiarsolan-2-yl)benzoic acid (**PhAs**).* Arsenic trioxide (250 mg, 1.3 mmol), anhydrous sodium carbonate (500 mg, 4.7 mmol), and copper sulfate pentahydrate (20 mg, 0.08 mmol) were suspended in 10 mL of H_2O. The mixture was heated at 80 °C until most of the solids had dissolved, and then, the solution was allowed to cool. 4-Aminobenzoic acid (274 mg, 2.0 mmol) was dissolved in 2 mL of DMF, and then, 0.25 mL of conc. HCl in a 10 mL ice−water mixture was added followed by addition of sodium nitrite solution (138 mg in 2 mL of H_2O, 2 mmol). The diazonium salt solution obtained was added slowly to the arsenite mixture at 0 °C for 1 h. The reaction mixture was stirred at room temperature for 12 h and acidized by conc. HCl to pH 2. Subsequently, the precipitate was filtered off and the filtrate was evaporated in vacuo[45] and extracted twice with 15 mL of DMF to eliminate most of the inorganic salt formed. The above filtrate was stirred with EDT (490 mg, 5.2 mmol) at room temperature for 2 h and finally purified by HPLC (a gradient elution was performed: starting from 95/5 H_2O/ACN to 10/90 H_2O/ACN in 25 min, 0.1% TFA, 5.0 mL/min) to yield **PhAs** (290 mg, 39%) as a white solid. ^{1}H NMR (500 MHz, DMSO-d_6): δ 13.56 (s, 1H), 7.93 (d, J = 8.1 Hz, 2H), 7.79 (d, J = 7.9 Hz, 2H), 3.21−2.84 (m, 2H). ^{13}C NMR (125 MHz, DMSO-d_6): δ 167.50, 150.38, 131.63, 131.31, 129.28, 42.05. HRMS (ESI): m/z Calcd for $C_9H_9AsO_2S_2$ $[M\text{-}H]^-$, 286.9187, found 286.9233 (Figure S4).

*Synthesis of (2-(3-(4-Amino-3-(4-phenoxyphenyl)-1H-pyrazolo-[3,4-d]pyrimidin-1-yl)piperidin-1-yl)-2-oxoethyl)arsonic Acid (**I-As-V**).* **As-V** (100 mg, 0.54 mmol), kinase-recognition scaffold (50 mg, 0.13 mmol), EDCI (207 mg, 1.08 mmol), NHS (75 mg, 0.65 mmol), and TEA (109 mg, 1.08 mmol) were dissolved in 10 mL of DMF. The reaction mixture was stirred at room temperature for 4 h. Subsequently, the reaction mixture was concentrated in vacuo and washed with H_2O three times. The precipitate was collected and dried in vacuo to yield **I-As-V** (43 mg, 60%) as a white solid. ^{1}H NMR (500 MHz, DMSO-d_6) δ 8.26 (d, J = 6.4 Hz, 1H), 7.67 (dd, J = 8.8, 2.5 Hz, 2H), 7.52−7.38 (m, 2H), 7.23−7.05 (m, 5H), 4.87 (m, 0.5H), 4.66 (m, 0.5H), 4.56 (br d, J = 12.1 Hz, 0.5H), 4.25 (br d, J = 13.2 Hz, 0.5H), 4.13 (br d, J = 9.7 Hz, 0.5H), 3.97 (br d, J = 13.5 Hz, 0.5H), 3.75 (m, 0.5H), 3.68 (d, J = 13.9 Hz, 1H), 3.50 (d, J = 14.2 Hz, 1H), 3.23−3.00 (m, 1H), 2.87 (m, 0.5H), 2.30−2.06 (m, 2H), 1.94−1.73 (m, 2H). ^{13}C NMR (125 MHz, DMSO-d_6) δ 163.07, 158.65, 157.60, 156.78, 156.11, 154.38, 143.89, 130.61, 128.36, 124.26, 119.44, 97.82, 55.39, 52.49, 50.66, 46.93, 46.08, 42.07, 29.96, 24.86, 23.75. HRMS (ESI): m/z Calcd for $C_{24}H_{25}AsN_6O_5$ $[M + H]^+$, 553.1175, found 553.1181 (Figure S5).

*Synthesis of 1-(3-(4-Amino-3-(4-phenoxyphenyl)-1H-pyrazolo-[3,4-d]pyrimidin-1-yl)piperidin-1-yl)-2-(1,3,2-dithiarsolan-2-yl)-ethan-1-one (**I-As-1**).* **As-V** (185 mg, 1 mmol), kinase-recognition scaffold (97 mg, 0.25 mmol), EDCI (382 mg, 2 mmol), NHS (138 mg, 1.2 mmol), and TEA (202 mg, mmol) were dissolved in 20 mL of DMF. The reaction mixture was stirred at room temperature for 4 h followed by the dropwise addition of EDT (94 mg, 1 mmol). After stirring at room temperature for 4 h, the mixture was purified by HPLC (a gradient elution was performed: starting from 95/5 H_2O/ACN to 10/90 H_2O/ACN in 25 min, 0.1% TFA, 5.0 mL/min) to yield **I-As-1** (116 mg, 78%) as a white solid.^{1}H NMR (500 MHz, $CDCl_3$): δ 8.26 (d, J = 20.4 Hz, 1H), 7.58 (d, J = 8.1 Hz, 2H), 7.46−7.36 (m, 2H), 7.24−7.13 (m, 3H), 7.09 (d, J = 8.0 Hz, 2H), 6.33 (br d, J = 24.4 Hz, 2H), 5.01−4.82 (m, 1H), 4.74 (br d, J = 12.7 Hz, 0.5H), 4.55 (br d, J = 13.3 Hz, 0.5H), 4.07 (br d, J = 17.3 Hz, 0.5H), 3.87 (br d, J = 13.5 Hz, 0.5H), 3.72 (m, 0.5H), 3.45−3.28 (m, 5H), 3.08−2.92 (m, 2H), 2.85 (m, 0.5H), 2.42−2.20 (m, 2H), 2.12−1.91 (m, 1H), 1.82−1.66 (m, 1H). ^{13}C NMR (125 MHz, $CDCl_3$): δ 169.31, 159.76, 155.75, 153.67, 151.56, 145.89, 130.15, 124.58, 119.92, 119.26, 97.09, 53.45, 50.75, 46.72, 45.65, 42.26, 41.38, 29.97, 25.02, 23.88. HRMS (ESI): m/z Calcd for $C_{26}H_{27}AsN_6O_2S_2$ $[M + H]^+$, 595.0926, found 595.0949 (Figure S6).

*Synthesis of 1-(3-(4-Amino-3-(4-phenoxyphenyl)-1H-pyrazolo-[3,4-d]pyrimidin-1-yl)piperidin-1-yl)-3-(1,3,2-dithiarsolan-2-yl)-propan-1-one (**I-As-2**).* **As-2** (48 mg, 0.2 mmol), kinase-recognition scaffold (76 mg, 0.2 mmol), EDCI (77 mg, 0.4 mmol), NHS (28 mg,

https://doi.org/10.1021/acs.jmedchem.3c02076
J. Med. Chem. 2024, 67, 5458−5472

0.24 mmol), and TEA (40 mg, 0.4 mmol) were dissolved in DMF (5 mL). The reaction mixture was stirred at room temperature for 4 h. The reaction mixture was purified by HPLC (a gradient elution was performed: starting from 95/5 H_2O/ACN to 10/90 H_2O/ACN in 25 min, 0.1% TFA, 5.0 mL/min) to yield **I-As-2** (72 mg, 59%) as a white solid. ^{1}H NMR (500 MHz, $CDCl_3$): δ 8.33 (d, J = 18.9 Hz, 1H), 7.64 (dd, J = 8.3, 5.4 Hz, 2H), 7.43−7.36 (m, 2H), 7.22−7.13 (m, 3H), 7.09 (d, J = 7.9 Hz, 2H), 5.97 (br s, 2H), 4.92−4.76 (m, 1.5H), 4.51 (br d, J = 13.4 Hz, 0.5H), 4.03 (br d, J = 9.1 Hz, 0.5H), 3.87 (br d, J = 13.3 Hz, 0.5H), 3.70 (m, 0.5H), 3.39−3.12 (m, 5H), 2.88−2.71 (m, 2H), 2.65 (m, 0.5H), 2.46−2.20 (m, 2H), 2.08−1.93 (m, 3H), 1.78−1.65 (m, 1H). ^{13}C NMR (125 MHz, $CDCl_3$): δ 171.39, 158.75, 157.73, 155.17, 154.10, 144.29, 130.03, 124.18, 119.63, 119.17, 98.55, 53.38, 49.87, 45.59, 42.16, 41.61, 31.99, 29.85, 25.51, 25.04, 23.89. HRMS (ESI): m/z Calcd for $C_{27}H_{29}AsN_6O_2S_2$ $[M + H]^+$, 609.1082, found 609.1117 (Figure S7).

*Synthesis of 1-(3-(4-Amino-3-(4-phenoxyphenyl)-1H-pyrazolo-[3,4-d]pyrimidin-1-yl)piperidin-1-yl)-4-(1,3,2-dithiarsolan-2-yl)-butan-1-one (**I-As-3**).* **As-3** (51 mg, 0.2 mmol), kinase-recognition scaffold (76 mg, 0.2 mmol), EDC (77 mg, 0.4 mmol), NHS (28 mg, 0.24 mmol), and TEA (40 mg, 0.4 mmol) were dissolved in 5 mL of DMF. The reaction mixture was stirred at room temperature for 4 h. The reaction mixture was purified by HPLC (a gradient elution was performed: starting from 95/5 H_2O/ACN to 10/90 H_2O/ACN in 25 min, 0.1% TFA, 5.0 mL/min) to yield **I-As-3** (70 mg, 56%) as a brown solid. ^{1}H NMR (500 MHz, $CDCl_3$): δ 8.37 (d, J = 22.6 Hz, 1H), 7.66 (dd, J = 8.4, 6.5 Hz, 2H), 7.45−7.38 (m, 2H), 7.22−7.15 (m, 3H), 7.11 (d, J = 7.9 Hz, 2H), 6.25−5.59 (br s, 2H), 4.91−4.79 (m, 1.5H), 4.58 (br d, J = 13.3 Hz, 0.5H), 4.05 (br d, J = 8.8 Hz, 0.5H), 3.88 (br d, J = 13.6 Hz, 0.5H), 3.75−3.64 (m, 1H), 3.36−3.26 (m, 5H), 3.16 (m, 0.5H), 2.93−2.71 (m, 1.5H), 2.53−2.21 (m, 5H), 2.06−1.81 (m, 3H). ^{13}C NMR (125 MHz, $CDCl_3$): δ 170.83, 158.71, 157.76, 156.34, 155.36, 144.19, 129.95, 124.15, 119.61, 119.17, 98.57, 53.48, 49.86, 45.73, 41.67, 36.88, 34.20, 31.46, 29.71, 25.48, 24.03, 21.60, 14.15. HRMS (ESI): m/z Calcd for $C_{28}H_{31}AsN_6O_2S_2$ $[M + H]^+$, 623.1239, found 623.1259 (Figure S8).

*Synthesis of (2-(3-(4-Amino-3-(4-phenoxyphenyl)-1H-pyrazolo-[3,4-d]pyrimidin-1-yl)piperidin-1-yl)-2-oxoethyl)arsonous Acid (**I-As-4**).* **I-As-V** (110 mg, 0.2 mmol) and glutathione (123 mg, 0.4 mmol) were dissolved in 15 mL of DMSO and 15 mL of H_2O followed by addition of 1 M NaOH solution to adjust the pH to 7−8. The reaction mixture was stirred at room temperature for 4 h to generate **I-As-4** and byproduct **I-As-SG$_2$** and then purified by HPLC (a gradient elution was performed: starting from 95/5 H_2O/ACN to 10/90 H_2O/ACN in 25 min, 0.1% TFA, 5.0 mL/min) to yield **I-As-4** (23 mg, 21%) as a white solid. ^{1}H NMR (500 MHz, DMSO-d_6): δ 8.40−8.20 (m, 1H), 7.67 (dt, J = 8.5, 1.8 Hz, 2H), 7.50−7.36 (m, 2H), 7.27−7.05 (m, 5H), 4.89 (m, 0.5H), 4.67 (m, 0.5H), 4.56 (m, 0.5H), 4.24 (m, 0.5H), 4.14 (m, 0.5H), 3.97 (m, 0.5H), 3.81−3.69 (m, 1H), 3.65−3.50 (m, 1.5H), 3.24−3.04 (m, 1H), 2.89 (s, 1H), 2.74 (s, 1H), 2.31−1.99 (m, 2H), 1.91−1.73 (m, 1.5H). ^{13}C NMR (125 MHz, DMSO-d_6): δ 162.79, 157.69, 156.76, 155.47, 154.20, 144.13, 130.61, 128.21, 124.28, 119.46, 97.80, 55.38, 52.57, 50.63, 46.93, 46.07, 42.07, 36.25, 29.92, 24.83. HRMS (ESI): m/z Calcd for $C_{24}H_{25}AsN_6O_4$ $[M + H]^+$, 537.1226, found 537.1251 (Figure S9).

*Synthesis of 1-(3-(4-Amino-3-(4-phenoxyphenyl)-1H-pyrazolo-[3,4-d]pyrimidin-1-yl)piperidin-1-yl)-2-(((2-hydroxyethyl)thio)-(methyl)arsanyl)ethan-1-one (**I-As-5**).* Cacodylic acid (1.0 g, 7.25 mmol) was dissolved in 48% aq. HBr (6 mL), and the solution was heated at 130 °C for 10 h. Then, the mixture was extracted with 30 mL of dichloromethane. The organic layer was evaporated in vacuo to get methylarsenic dibromide.[46] A round-bottom flask was added with methylarsenic dibromide, sodium hydroxide (1.6 g), chloroacetic acid (685 mg, 7.25 mmol), and 10 mL of H_2O. The reaction mixture was stirred at room temperature for 5 h and then neutralized with conc. HCl to pH 2. Subsequently, the solvent was removed by evaporation, and the residue (**As^V-5**) was dissolved in 20 mL of DMF followed by adding the kinase-recognition scaffold (100 mg, 0.26 mmol), EDCI (400 mg, 2 mmol), NHS (150 mg, 1.3 mmol), and TEA (80 mg, 0.8 mmol). The reaction mixture was stirred at room temperature for 4 h and then purified by HPLC to yield **I-As^V-5**. **I-As^V-5** and mercaptoethanol (285 mg, 3.65 mmol) were dissolved in 10 mL of DMF. The reaction mixture was stirred at room temperature for 4 h and then purified by HPLC (a gradient elution was performed: starting from 95/5 H_2O/ACN to 10/90 H_2O/ACN in 25 min, 0.1% TFA, 5.0 mL/min) to yield **I-As-5** (30 mg, 19%) as a white solid powder. ^{1}H NMR (500 MHz, DMSO-d_6): δ 8.26 (d, J = 10.1 Hz, 1H), 7.66 (dd, J = 8.5, 3.3 Hz, 2H), 7.44 (t, J = 7.8 Hz, 2H), 7.22−7.09 (m, 5H), 4.89−4.77 (m, 1H), 4.71−4.60 (m, 0.5H), 4.51 (m, 0.5H), 4.29−4.06 (m, 0.5H), 4.05−3.94 (m, 0.5H), 3.56−3.42 (m, 2H), 3.26−3.04 (m, 2H), 3.01−2.79 (m, 2H), 2.77−2.60 (m, 2H), 2.23 (m, 1H), 2.17−2.06 (m, 1H), 2.00−1.82 (m, 1H), 1.37−1.24 (m, 3H). ^{13}C NMR (125 MHz, DMSO-d_6): δ 163.77, 158.69, 157.62, 156.79, 156.16, 154.41, 143.88, 130.62, 128.38, 124.28, 119.45, 97.85, 63.40, 60.03, 52.54, 46.96, 46.08, 41.60, 33.68, 29.98, 24.85, 18.78, 14.48. HRMS (ESI): m/z Calcd for $C_{27}H_{31}AsN_6O_3S$ $[M + H]^+$, 595.1467, found: 595.1523 (Figure S10).

*Synthesis of 1-(3-(4-Amino-3-(4-phenoxyphenyl)-1H-pyrazolo-[3,4-d]pyrimidin-1-yl)piperidin-1-yl)-2-(dimethylarsanyl)ethan-1-one (**I-As-Me$_2$**).* Cacodylic acid (1.0 g, 7.25 mmol) was dissolved in 48% aq. HBr (6.0 mL), and the solution was stirred at room temperature for 3 h.[46] The mixture was evaporated, and sodium hydroxide (1.6 g), chloroacetic acid (685 mg, 7.25 mmol), and 10 mL of H_2O were added. The reaction mixture was stirred at room temperature for 5 h and then neutralized with conc. HCl to pH 2. Subsequently, the solvent was removed by evaporation, and the residue (**As^V-Me$_2$**) was dissolved in 20 mL of DMF followed by adding kinase-recognition scaffold (100 mg, 0.26 mmol), EDCI (400 mg, 2 mmol), NHS (150 mg, 1.3 mmol), and TEA (80 mg, 0.8 mmol). The reaction mixture was stirred at room temperature for 4 h and then purified by HPLC to yield **I-As^V-Me$_2$**. **I-As^V-Me$_2$** and mercaptoethanol (285 mg, 3.65 mmol) were dissolved in 10 mL of DMF. The reaction mixture was stirred at room temperature for 4 h and then purified by HPLC (a gradient elution was performed: starting from 95/5 H_2O/ACN to 10/90 H_2O/ACN in 25 min, 0.1% TFA, 5.0 mL/min) to yield **I-As-Me$_2$** (22 mg, 16%) as a white solid powder. ^{1}H NMR (500 MHz, DMSO-d_6): δ 8.35 (s, 1H), 7.67 (dd, J = 8.8, 2.5 Hz, 2H), 7.52−7.39 (m, 2H), 7.31−7.10 (m, 5H), 4.78 (m, 0.5H), 4.63 (m, 0.5H), 4.54 (br d, J = 12.0 Hz, 0.5H), 4.30 (br d, J = 13.0 Hz, 0.5H), 4.15 (br d, J = 13.5 Hz, 0.5H), 3.96 (br d, J = 13.5 Hz, 0.5H), 3.68−3.63 (m, 1.5H), 3.22−3.08 (m, 1H), 2.79 (m, 0.5H), 2.13−2.08 (m, 2H), 1.96−1.87 (m, 2H), 1.07−0.90 (m, 6H). ^{13}C NMR (125 MHz, DMSO-d_6): δ 163.25, 158.70, 157.62, 156.80, 156.16, 154.41, 143.89, 130.62, 128.39, 124.28, 119.45, 97.85, 52.53, 50.69, 46.95, 46.08, 42.09, 29.97, 24.85, 23.74, 18.77. HRMS (ESI): m/z Calcd for $C_{26}H_{29}AsN_6O_2$ $[M + Na]^+$, 555.1460, found: 555.1501 (Figure S11).

*Synthesis of (4-(1,3,2-Dithiarsolan-2-yl)phenyl)(3-(4-amino-3-(4-phenoxyphenyl)-1H-pyrazolo[3,4-d]pyrimidin-1-yl)piperidin-1-yl)-methanone (**I-PhAs**).* **PhAs** (57 mg, 0.2 mmol), kinase-recognition scaffold (76 mg, 0.2 mmol), EDCI (77 mg, 0.4 mmol), NHS (28 mg, 0.24 mmol), and TEA (40 mg, 0.4 mmol) were dissolved in 5 mL of DMF. The reaction mixture was stirred at room temperature for 4 h and then purified by HPLC (a gradient elution was performed: starting from 95/5 H_2O/ACN to 10/90 H_2O/ACN in 25 min, 0.1% TFA, 5.0 mL/min) to yield **I-PhAs** (85 mg, 65%) as a brown solid. ^{1}H NMR (500 MHz, $CDCl_3$): δ 8.29 (br s, 1H), 7.72 (br s, 2H), 7.58 (br s, 2H), 7.49−7.35 (m, 4H), 7.26−7.22 (m, 1H), 7.19 (d, J = 8.7 Hz, 2H), 7.12 (d, J = 8.0 Hz, 2H), 6.32 (s, 2H), 5.18−4.51 (m, 2H), 3.86−3.58 (m, 1.5H), 3.46−3.36 (m, 2H), 3.27−3.08 (m, 3H), 3.05−2.94 (m, 0.5H), 2.50−2.21 (m, 2H), 2.20−1.94 (m, 1H), 1.90−1.54 (m, 1H). ^{13}C NMR (125 MHz, $CDCl_3$): δ 170.53, 163.08, 159.85, 155.69, 153.63, 151.59, 147.03, 146.57, 145.96, 135.67, 130.94, 130.15, 129.74, 126.83, 125.03, 124.61, 119.94, 119.22, 97.12, 42.02, 37.01, 31.90, 30.03, 24.58. HRMS (ESI): m/z Calcd for $C_{31}H_{29}AsN_6O_2S_2$ $[M + H]^+$, 657.1082, found 657.1087 (Figure S12).

Kinase Enzymology Assays. BTK recombinant protein (cat. no. 10578-H08B) was purchased from Sino Biological (China). Kinase enzymology assays were performed according to the protocols specified in HTRF KinEaseTM assays (Cisbio Bioassays, France).

https://doi.org/10.1021/acs.jmedchem.3c02076
J. Med. Chem. 2024, 67, 5458−5472

Briefly, BTK (10 ng) and substrate (1 μM) were mixed with various concentrations of inhibitors (DMSO, 0.5%) at room temperature for 30 min followed by addition of ATP (200 μM) to start enzymatic reactions. After 1 h, the reactions were stopped by EDTA detection solution, and then, europilated antiphosphotyrosine antibodies and streptavidin XL665 (125 nM) conjugates were added. The mixtures were incubated at room temperature for another 1 h and read by a plate reader (Tecan spark, Switzerland). Data analysis was performed with GraphPad Prism 7.0.

In Situ Assays Evaluating the Reactivity of As Inhibitors. Ramos cells (ATCC) and OCI-LY10 (Beijing Biobw Biological Technology, Beijing, China) were cultured in RPMI 1640 medium (cat. no. 01-100-1A, BioInd) containing 10% heat-inactivated fetal bovine serum (cat. no. 04-001-1A, Bioind) and 100 units/mL penicillin-streptomycin (cat. no. 03-031-1B, BioInd) and cultured in a humidified 37 °C incubator with 5% CO_2. Dimethyl sulfoxide (DMSO, cat. no. D2650) was purchased from Sigma-Aldrich (USA). PCI-33380 (cat. no. HY-100335) was purchased from MedChemExpress (USA).

The concentration-dependent reactivity of inhibitors toward BTK in Ramos cells (6×10^6, 2 mL) was assessed by preincubating the cells with increasing concentrations of **I-As-1**, **2**, **3**, **4**, **5**, **Me_2**, **V**, **I-PhAs**, guiding group alone, nontargeted arsenicals (**As-2**, **As-3**, **As-V**, **PhAs**, **iAs^{III}**, **MMA^{III}**, and **DMA^{III}**), or ibrutinib for 1 h followed by the labeling with PCI-33380 (2 μM, 1 h), which is a Bodipy-FL fluorophore-modified ibrutinib derivative that is able to bind specifically with BTK (Figure S14).[49] Cells were washed with PBS three times to remove FBS proteins as well as excess probes, and the pellets were lysed directly in RIPA buffer (cat. no. R0010, Beyotime). The lysates were cleared by centrifugation at 13,000*g* for 10 min at 4 °C and normalized by the BCA assay (cat. no. P0012, Beyotime). Samples were then heated at 95 °C for 10 min, resolved by SDS-polyacrylamide gels (12%), and visualized by fluorescent gel scanning using a GE (AI600, USA) scanner (Ex, 460 nm; Em, Cy2 Filter). The proteins in the gels after scanning were transferred to poly-(vinylidenedifluoride) membranes using a Trans-Blot Turbo Transfer system (Bio-Rad, USA). Total BTK was detected by standard Western blotting techniques using a specific anti-BTK antibody (cat. no. 8547, Cell signaling).

Molecular Docking Analysis. AutoDock (version 4.2.6) was used to perform the docking analysis. The crystal structure (PDB ID: 5P9J) was obtained from the Protein Data Bank.[50] The structure contains the ibrutinib ligand. We deleted the ligand and water molecules from the structure and added hydrogens for the receptor with PyMOL (version 2.5.4). The arsenic-based targeting inhibitors (As inhibitors, **I-As-1**, **2**, **3**, **4**, **5**, and **I-PhAs**) were designed with ChemDraw (version 14.0) and converted into a 3D structure with Openbabel (version 2.4.1). Each As atom in these ligands was covalently connected to a sulfur atom, and the length of the As−S bond was set as 2.27 Å (Angstrom) in Discovery Studio Visualizer (version 21.1.0.20298). We connected each ligand to residue Cys481 in BTK with *prepareCovalent.py* from package adCovalentDockResidue (version 1.2),[65] generating a pdb file that contained Cys481 and the ligand. Because there are no parameters for arsenic atoms in the default AD4.1_bound.dat file, we manually updated the AD4.1_bound.dat file by adding line: "atom_par As 4.23 0.309 13.000 -0.00110 0.0 0.0 0 -1 -1 4" according to the AutoDock User-Guide. The pdbqt files of the receptor and the ligands were then generated with *prepare_receptor* in ADFRsuite (version 1.0). These pdbqt files of ligands and receptor were processed by *prepare_flexreceptor4.py*, in which the Cys481 was set as the flexible side chain. The gpf and dpf files were generated by *prepare_gpf4.py* and *prepare_dpf4.py* from MGLTools package for each docking, respectively. The "spacing" parameter was set as 0.500. The times of running was set as 50. Other parameters were all default settings. To ensure the validity of docking, the line "rmsdatoms all" was added to the gpf files, and the line "unbound_model bound" in dpf files has to be replaced by "unbound_energy 0.0". The line "parameter_file AD4.1_bound.dat" was added to both gpf and dpf files to provide parameters of the As atom. The griding and docking were then processed by autogrid4 and autodock4 in AutoDock. The docking results were visualized by using PyMOL (Figure S14 and Table S1).

BCR Signaling Pathway Inhibition Study. Ramos cells (6×10^6, 2 mL) were preincubated with varying concentrations of inhibitors for 1 h, washed three times with PBS, and then stimulated with anti-IgM (20 μg/mL, cat. no. SA103, Solarbio) for 10 min. Cells were lysed directly in RIPA buffer (cat. no. R0010, Beyotime). The lysates were cleared by centrifugation at 13,000*g* for 10 min at 4 °C and normalized by the BCA assay (cat. no. P0012, Beyotime). Samples were heated at 95 °C for 10 min and analyzed by Western blot using phospho-specific antibodies Phospho-Syk (Tyr525/526, cat. no. 2710, Cell signaling), Phospho-BTK (Tyr223, cat. no. 5082, Cell signaling), Phospho-PLCγ2 (Tyr1217, cat. no. 3871, Cell signaling), Phospho-p44/42 MAPK (Erk1/2) (Thr202/Tyr204, cat. no. 4370, Cell signaling). Chemiluminescence detection (cat. no. 35071, Thermo Fisher Scientific) was then performed. Blots were then stripped and reprobed with antibodies that specifically bind with Syk (cat. no. 2712, Cell signaling), BTK (cat. no. 8547, Cell signaling), PLCγ2 (cat. no. 3872, Cell signaling), Erk (cat. no. 4695, Cell signaling), and β-actin (cat. no. 4970, Cell signaling) to detect the respective protein levels.

Cell Viability and Uptake Assays. Ramos cells were seeded in 96-well plates (10,000 cells/well), incubated for 12 h, then treated with inhibitors (0.5% DMSO) for 72 h, and measured with a Cell Counting Kit-8 (cat. no. C0038, Beyotime). Data analysis was performed with GraphPad Prism 7.0 (Table S2).

Cell uptake assays of As inhibitors. Ramos cells (6×10^6 cells, 2 mL) were treated with the indicated concentrations of inhibitors for 1 h (DMSO, 0.5%). Cells were washed with PBS three times. Then, cells were harvested by centrifugation. The cell pellets were digested with 10% HNO_3 in a 60 °C water bath overnight. Then, the digested solution was diluted 5 times with deionized water and filtered through a 0.45 μm membrane filter. The concentration of arsenic in the filtrated was measured by ICPMS.

Cell uptake assays of ibrutinib. Ramos cells (6×10^6 cells, 2 mL) were treated with the indicated concentrations of ibrutinib for 1 h (DMSO, 0.5%). Cells were washed with PBS three times. Then, cells were harvested by centrifugation. The cell pellets were repeatedly subjected to freeze−thaw and resuspended in dimethyl sulfoxide (DMSO, 0.2 mL) and sonicated for 10 min with an ice bath. Then, the extracted solution was filtered through a 0.45 μm membrane filter. The concentration of ibrutinib in the filtrated was measured by HPLC-ESIMS and quantified through a calibration curve.

Mass Spectrometry Study of the Binding of Inhibitors with BTK. BTK was labeled with inhibitors under the following conditions: 10 μL of 0.36 mg/mL BTK and 10 μL of 15 μM inhibitors in 10% DMSO were added to 200 μL of NH_4HCO_3 buffer (100 mM NH_4HCO_3, pH 8.0, 1 mM $ZnCl_2$, 1 mM DTT) and incubated at room temperature for 1 h. BTK covalent competitive occupancy was assessed by preincubation with inhibitors for 1 h before labeling with ibrutinib for 10 min. After the labeling, protein samples were reduced with 10 mM DTT for 30 min at 30 °C and alkylated with iodoacetamide (20 mM) in the dark for 30 min at room temperature. Protein samples were then digested with trypsin (cat. no. P8101S, NEB) at a ratio of 1/20 (enzyme/protein) for 15 h at 37 °C. The digested peptides were analyzed with a UitiMate 3000 RSLCnano system with a BEH C18 column coupled to a Bruker Impact II ESI-Q-TOF-MS with a CaptiveSpray source (ion polarity, positive; mass range, 150−2200 m/z; scan mode, AutoMS/MS; capillary voltage, 1300 V; nanobooster, 0.2 bar; dry gas, 3 L/min; dry temperature, 150 °C).

Cellular Washout Experiment. Ramos cells (6×10^6, 2 mL) were preincubated with cycloheximide (5 μg/mL) for 30 min at 37 °C. Cells were washed with PBS three times to remove cycloheximide and returned to culture. Ibrutinib, **I-As-1**, or **I-As-Me_2** were added to a final concentration of 1 μM and incubated at 37 °C for 1 h. Cells were washed with PBS three times and then incubated in fresh medium at 37 °C for 0, 4, or 20 h. Subsequently, the cells were treated with PCI-33380 (2 μM) for 1 h and then washed with PBS three times to remove excess probes. Cell pellets after centrifugation were

https://doi.org/10.1021/acs.jmedchem.3c02076
J. Med. Chem. 2024, 67, 5458−5472

lysed directly in RIPA buffer (cat. no. R0010, Beyotime). The lysates were cleared by centrifugation at 13,000*g* for 10 min at 4 °C and normalized by the BCA assay (cat. no. P0012, Beyotime). Samples were heated at 95 °C for 10 min and analyzed by SDS-polyacrylamide gels (12%) and fluorescent gel scanning using a GE (AI600, USA) scanner (Ex, 460 nm; Em, Cy2 Filter). The proteins in the gels after scanning were transferred to poly(vinylidenedifluoride) membranes using a Trans-Blot Turbo Transfer system (Bio-Rad, USA). Total BTK was detected by standard Western blotting techniques using a specific anti-BTK antibody (cat. no. 8547, Cell signaling).

Selectivity of the As Inhibitor. Ramos cells were labeled with 2−20 μM PCI33380 and then analyzed by SDS-polyacrylamide gels (12%) and fluorescent gel scanning to reveal the target and off-target fluorescence band (Figure S13). Ramos cells (6×10^6, 2 mL) were incubated with increasing concentrations of PCI-33380 (2−20 μM) for 1 h and then washed with PBS three times to remove serum proteins and excess probes. Cell pellets after centrifugation were lysed directly in RIPA buffer (cat. no. R0010, Beyotime). The lysates were cleared by centrifugation at 13,000*g* for 10 min at 4 °C and normalized by the BCA assay (cat. no. P0012, Beyotime). Samples were heated at 95 °C for 10 min and analyzed by SDS-polyacrylamide gels (12%) and fluorescent gel scanning using a GE (AI600, USA) scanner (Ex, 460 nm; Em, Cy2 Filter). The proteins in the gels after scanning were transferred to poly(vinylidenedifluoride) membranes using a Trans-Blot Turbo Transfer system (Bio-Rad, USA). Total BTK was detected by standard Western blotting techniques using a specific anti-BTK antibody (cat. no. 8547, Cell signaling).

To evaluate the selectivity of **I-As-1** in Ramos cells, we conducted a concentration-dependent competition labeling experiment using a high concentration of PCI-33380 (20 μM) to trace the nonspecific binding with off-target proteins. Ramos cells (6×10^6, 2 mL) were first incubated with increasing concentrations of **I-As-1** or ibrutinib (0.001−20 μM) for 1 h followed by labeling with PCI-33380 (20 μM, 1 h). Cells were then washed with PBS three times to remove FBS proteins and excess probes, and the cell pellets after centrifugation were lysed directly in RIPA buffer (cat. no. R0010, Beyotime). The lysates were cleared by centrifugation at 13,000*g* for 10 min at 4 °C and normalized by the BCA assay (cat. no. P0012, Beyotime). Samples were heated at 95 °C for 10 min and analyzed by SDS-polyacrylamide gels (12%) and fluorescent gel scanning using a GE (AI600, USA) scanner (Ex, 460 nm; Em, Cy2 Filter). The proteins in the gels after scanning were transferred to poly(vinylidenedifluoride) membranes using a Trans-Blot Turbo Transfer system (Bio-Rad, USA). Total BTK was detected by standard Western blotting techniques using a specific anti-BTK antibody (cat. no. 8547, Cell signaling).

***In Vivo* Efficacy and *In Vivo* Biodistribution of I-As-1.** Female severe combined immunodeficiency disease (SCID) mice were injected subcutaneously with 5×10^6 OCI-LY10 cells. When xenograft tumors' volume reached approximately 100 mm^3 that could be clearly observed and measured, mice were randomized into four groups (n = 5/group) and treated with vehicle, **I-As-1**, ibrutinib, and nontargeted arsenical (**As-2**) through tail vein injection once a day. Inhibitors (20 μmol/kg) were administered via the tail vein as a clear solution in an optimized vehicle (87.5% saline, 10% Solutol HS 15, 2.5% DMSO). Tumor size (tumor volume = length × width^2 × 0.52) and body weight were monitored periodically for 14 days. When the tumor volume of the any group reached an intolerable size >2000 mm^3, the treatment was ended and the mice were euthanized. Statistical analysis was conducted by one-way ANOVA. Two-tailed Student's t test was used to analyze the statistical significance between each treatment group and the vehicle group. $P < 0.01$ is considered as statistically significant. At the end of treatment, mice were sacrificed and the *in vivo* distribution of the As inhibitor in different organs was studied through quantifying arsenic by ICP-MS (Figure S16). Excised organs and tumors were digested with 65% HNO_3 in a 150 °C graphite block digester (SPB 50−24, PerkinElmer) overnight. Then, the digested solution was diluted with 2% HNO_3 and filtered through a 0.45 μm membrane filter. The concentration of arsenic in the filtrated was measured by ICPMS. All animal experiments were approved by the Xiamen University Laboratory Animal Center (approval code: XMULAC20210079) and were performed in accordance with the guidelines of the Xiamen University Institutional Committee for the Care and Use of Laboratory Animals.

***In Vivo* Pharmacokinetic Study.** Ibrutinib and **I-As-1** were administered via intravenous injection at a dose of 20 μmol/kg to evaluate their pharmacokinetics in ICR mice (n = 3). Blood samples of approximately 30−50 μL were collected from each mouse at 5, 15, 30, 60, 120, 240, and 480 min following the administration of ibrutinib or **I-As-1**. The blood samples were then centrifuged at 12,000*g* for 10 min, and the supernatant plasma was collected. The concentration of ibrutinib in the plasma was measured by HPLC-ESIMS and quantified through a calibration curve, and the concentration of arsenic in the plasma was measured by ICPMS. The binding of **I-As-1** to plasma proteins and its release after the addition of 10 mM EDT were analyzed by SEC-ICPMS.

■ ASSOCIATED CONTENT

Supporting Information

The Supporting Information is available free of charge at https://pubs.acs.org/doi/10.1021/acs.jmedchem.3c02076.

General considerations and experimental procedures and additional figures and tables (^{1}H NMR, ^{13}C NMR, and HRMS spectra of compounds, in situ reactivity of inhibitors, binding mode and energy comparison of As inhibitors and ibrutinib with BTK, BCR signaling pathway inhibition study, IC_{50} values of inhibitors against Ramos, OCI-LY10, or HepG2 cells and the cell uptake of inhibitors, retention time of As inhibitors and ibrutinib in RPLC, schematic illustration evaluating the reversibility of covalent bonding between inhibitors and BTK, reversible covalent nature of As inhibitors demonstrated by the peptide mapping experiment and cellular washout experiment, in situ assays evaluating the selectivity of the As inhibitor, potency of **I-As-1** toward BTK in OCI-LY10 cells, *in vivo* biodistribution of **I-As-1**, *in vivo* pharmacokinetic study, HPLC traces for reactive As inhibitors) (PDF)

Molecular formula strings (CSV)

■ AUTHOR INFORMATION

Corresponding Author

Xiaowen Yan − *Department of Chemistry and the MOE Key Laboratory of Spectrochemical Analysis & Instrumentation, College of Chemistry and Chemical Engineering, Xiamen University, Xiamen 361005, China; Innovation Laboratory for Sciences and Technologies of Energy Materials of Fujian Province (IKKEM), Xiamen 361005, China;* orcid.org/0000-0001-6608-6044; Email: xwyan@xmu.edu.cn

Authors

Yang Zhao − *Department of Chemistry and the MOE Key Laboratory of Spectrochemical Analysis & Instrumentation, College of Chemistry and Chemical Engineering, Xiamen University, Xiamen 361005, China*

Xinyue Zhao − *Department of Chemistry and the MOE Key Laboratory of Spectrochemical Analysis & Instrumentation, College of Chemistry and Chemical Engineering, Xiamen University, Xiamen 361005, China*

Lewei Duan − *Laboratory of Epigenetics at Institutes of Biomedical Sciences and Intelligent Medicine Institute, Fudan University, Shanghai 200032, China*

Ruxue Hou − *Department of Chemistry and the MOE Key Laboratory of Spectrochemical Analysis & Instrumentation,*

College of Chemistry and Chemical Engineering, Xiamen University, Xiamen 361005, China

Yuxin Gu − *Department of Chemistry and the MOE Key Laboratory of Spectrochemical Analysis & Instrumentation, College of Chemistry and Chemical Engineering, Xiamen University, Xiamen 361005, China*

Zhen Liu − *Department of Chemistry and the MOE Key Laboratory of Spectrochemical Analysis & Instrumentation, College of Chemistry and Chemical Engineering, Xiamen University, Xiamen 361005, China*

Jianbin Chen − *Department of Chemistry and the MOE Key Laboratory of Spectrochemical Analysis & Instrumentation, College of Chemistry and Chemical Engineering, Xiamen University, Xiamen 361005, China*

Feizhen Wu − *Laboratory of Epigenetics at Institutes of Biomedical Sciences and Intelligent Medicine Institute, Fudan University, Shanghai 200032, China; Key Laboratory of Birth Defects, Children's Hospital of Fudan University, Shanghai 201102, China*

Limin Yang − *Department of Chemistry and the MOE Key Laboratory of Spectrochemical Analysis & Instrumentation, College of Chemistry and Chemical Engineering, Xiamen University, Xiamen 361005, China*

X. Chris Le − *Division of Analytical and Environmental Toxicology, Department of Laboratory Medicine and Pathology, University of Alberta, Edmonton, Alberta T6G 2G3, Canada;* orcid.org/0000-0002-7690-6701

Qiuquan Wang − *Department of Chemistry and the MOE Key Laboratory of Spectrochemical Analysis & Instrumentation, College of Chemistry and Chemical Engineering, Xiamen University, Xiamen 361005, China;* orcid.org/0000-0002-5166-4048

Complete contact information is available at: https://pubs.acs.org/10.1021/acs.jmedchem.3c02076

Author Contributions

X.Y. conceived the project and supervised research design and details. Y.Z. designed and conducted all the experiments. X.Z. participated in the chemical synthesis. F.W. and L.D. performed the molecular docking study. R.H., Y.G., and Z.L. participated in the biochemistry experiments. J.C. provided technical support. L.Y., X.C.L., and Q.W. offered constructive suggestions for the improvement of this work. The manuscript was initially prepared by Y.Z. and revised by X.Y.

Notes

The authors declare no competing financial interest.

■ ACKNOWLEDGMENTS

This study was financially supported by the National Natural Science Foundation of China (22074127, 22193053), the National Key Research and Development Program of China (2022YFF0710200), the Science and Technology Projects of Innovation Laboratory for Sciences and Technologies of Energy Materials of Fujian Province (IKKEM) (HRTP-[2022]-13), and the Fundamental Research Funds for the Central Universities (20720200073). Molecular docking analysis was supported by the Medical Research Data Center of Fudan University.

■ ABBREVIATIONS USED

APL, acute promyelocytic leukemia; ACN, acetonitrile; BTK, Bruton's tyrosine kinase; BCR, B-cell receptor; CAM, carbamidomethyl; DMA^{III}, dimethylarsinous acid; EDT, ethane-1,2-dithiol; ESIMS, electrospray ionization mass spectrometry; EDCI, 1-ethyl-3-(3-dimethyllaminopropyl) carbodiimide hydrochloride; Erk1/2, extracellular regulated kinase 1/2; GSAO, glutathione arsenoxide; HOBT, 1-hydroxybenzotriazole; iAs^{III}, sodium arsenite; IAA, iodoacetamide; ICPMS, inductively coupled plasma mass spectrometry; MMA^{III}, monomethylarsonous acid; NHS, *N*-hydroxysuccinimide; PLCγ2, phosphoinositide-specific phospholipase C gamma2; PML-RARα, promyelocytic leukemia-retinoic acid receptor alpha; RPLC, reverse-phase liquid chromatography; Syk, spleen tyrosine kinase; SEC, size-exclusion chromatography; TEA, triethylamine

■ REFERENCES

(1) Dilda, P. J.; Hogg, P. J. Arsenical-based cancer drugs. *Cancer Treat. Rev.* **2007**, *33* (6), 542−564.

(2) Chen, B. B.; Liu, Q. Q.; Popowich, A.; Shen, S. W.; Yan, X. W.; Zhang, Q.; Li, X. F.; Weinfeld, M.; Cullen, W. R.; Le, X. C. Therapeutic and analytical applications of arsenic binding to proteins. *Metallomics* **2015**, *7* (1), 39−55.

(3) Williams, K. J. The introduction of 'chemotherapy' using arsphenamine-the first magic bullet. *J. R. Soc. Med.* **2009**, *102* (8), 343−348.

(4) Zaffiri, L.; Gardner, J.; Toledo-Pereyra, L. H. History of Antibiotics. From Salvarsan to Cephalosporins. *J. Invest. Surg.* **2012**, *25* (2), 67−77.

(5) Wang, Z. G.; Rivi, R.; Delva, L.; Konig, A.; Scheinberg, D. A.; Gambacorti-Passerini, C.; Gabrilove, J. L.; Warrell, R. P.; Pandolfi, P. P. Arsenic trioxide and melarsoprol induce programmed cell death in myeloid leukemia cell lines and function in a PML and PML-RAR alpha independent manner. *Blood* **1998**, *92* (5), 1497−1504.

(6) Don, A. S.; Kisker, O.; Dilda, P.; Donoghue, N.; Zhao, X. Y.; Decollogne, S.; Creighton, B.; Flynn, E.; Folkman, J.; Hogg, P. J. A peptide trivalent arsenical inhibits tumor angiogenesis by perturbing mitochondrial function in angiogenic endothelial cells. *Cancer Cell* **2003**, *3* (5), 497−509.

(7) Golemovic, M.; Quintas-Cardama, A.; Manshouri, T.; Orsolic, N.; Duzkale, H.; Johansen, M.; Freireich, E. J.; Kantarjian, H.; Zingaro, R. A.; Verstovsek, S. MER1, a novel organic arsenic derivative, has potent PML-RAR alpha- independent cytotoxic activity against leukemia cells. *Invest. New Drug.* **2010**, *28* (4), 402−412.

(8) Mann, K. K.; Wallner, B.; Lossos, I. S.; Miller, W. H. Darinaparsin: a novel organic arsenical with promising anticancer activity. *Expert Opin. Inv. Drug.* **2009**, *18* (11), 1727−1734.

(9) Swindell, E. P.; Hankins, P. L.; Chen, H. M.; Miodragovic, D. U.; O'Halloran, T. V. Anticancer Activity of Small-Molecule and Nanoparticulate Arsenic(III) Complexes. *Inorg. Chem.* **2013**, *52* (21), 12292−12304.

(10) Akhtar, A.; Wang, S. X.; Ghali, L.; Bell, C.; Wen, X. Recent advances in arsenic trioxide encapsulated nanoparticles as drug delivery agents to solid cancers. *J. Biomed. Res.* **2017**, *31* (3), 177−188.

(11) Sonksen, M.; Kerl, K.; Bunzen, H. Current status and future prospects of nanomedicine for arsenic trioxide delivery to solid tumors. *Med. Res. Rev.* **2022**, *42* (1), 374−398.

(12) Wang, Q. Q.; Jiang, Y.; Naranmandura, H. Therapeutic strategy of arsenic trioxide in the fight against cancers and other diseases. *Metallomics* **2020**, *12* (3), 326−336.

(13) Zhang, X. W.; Yan, X. J.; Zhou, Z. R.; Yang, F. F.; Wu, Z. Y.; Sun, H. B.; Liang, W. X.; Song, A. X.; Lallemand-Breitenbach, V.; Jeanne, M.; Zhang, Q. Y.; Yang, H. Y.; Huang, Q. H.; Zhou, G. B.; Tong, J. H.; Zhang, Y.; Wu, J. H.; Hu, H. Y.; de The, H.; Chen, S. J.; Chen, Z. Arsenic Trioxide Controls the Fate of the PML-RAR alpha Oncoprotein by Directly Binding PML. *Science* **2010**, *328* (5975), 240−243.

(14) Dethe, H.; Chomienne, C.; Lanotte, M.; Degos, L.; Dejean, A. The t(15;17) translocation of acute promyelocytic leukemia fuses the retinoic acid receptor alpha gene to a novel transcribed locus. *Nature* **1990**, *347* (6293), 558−561.
(15) Bercier, P.; Wang, Q. Q.; Zang, N.; Zhang, J.; Yang, C.; Maimaitiyiming, Y.; Abou-Ghali, M.; Berthier, C.; Wu, C.; Niwa-Kawakita, M.; Dirami, T.; Geoffroy, M. C.; Ferhi, O.; Quentin, S.; Benhenda, S.; Ogra, Y.; Gueroui, Z.; Zhou, C.; Naranmandura, H.; de The, H.; Lallemand-Breitenbach, V. Structural Basis of PML-RARA Oncoprotein Targeting by Arsenic Unravels a Cysteine Rheostat Controlling PML Body Assembly and Function. *Cancer. Discovery* **2023**, *13* (12), 2548−2565.
(16) Shen, S. W.; Li, X. F.; Cullen, W. R.; Weinfeld, M.; Le, X. C. Arsenic Binding to Proteins. *Chem. Rev.* **2013**, *113* (10), 7769−7792.
(17) Zhang, H.; Yan, W.; Aebersold, R. Chemical probes and tandem mass spectrometry: a strategy for the quantitative analysis of proteomes and subproteomes. *Curr. Opin. Chem. Biol.* **2004**, *8* (1), 66−75.
(18) Lu, J.; Chew, E. H.; Holmgren, A. Targeting thioredoxin reductase is a basis for cancer therapy by arsenic trioxide. *P. Natl. Acad. Sci. U.S.A.* **2007**, *104* (30), 12288−12293.
(19) Kitchin, K. T.; Wallace, K. The role of protein binding of trivalent arsenicals in arsenic carcinogenesis and toxicity. *J. Inorg. Biochem.* **2008**, *102* (3), 532−539.
(20) Zhang, L.; Duan, D.; Liu, Y.; Ge, C.; Cui, X.; Sun, J.; Fang, J. Highly selective off-on fluorescent probe for imaging thioredoxin reductase in living cells. *J. Am. Chem. Soc.* **2014**, *136* (1), 226−233.
(21) Yan, X. W.; Li, J. H.; Liu, Q. Q.; Peng, H. Y.; Popowich, A.; Wang, Z. X.; Li, X. F.; Le, X. C. p-Azidophenylarsenoxide: An Arsenical ″Bait″ for the In Situ Capture and Identification of Cellular Arsenic-Binding Proteins. *Angew. Chem., Int. Ed.* **2016**, *55* (45), 14051−14056.
(22) Chen, S.; Wu, J. L.; Liang, Y.; Tang, Y. G.; Song, H. X.; Wu, L. L.; Xing, Y. F.; Yan, N.; Li, Y. T.; Wang, Z. Y.; Xiao, S. J.; Lu, X.; Chen, S. J.; Lu, M. Arsenic Trioxide Rescues Structural p53 Mutations through a Cryptic Allosteric Site. *Cancer Cell* **2021**, *39* (2), 225−239.
(23) Hu, X. Q.; Li, H. Y.; Ip, T. K. Y.; Cheung, Y. F.; Koohi-Moghadam, M.; Wang, H. B.; Yang, X. M.; Tritton, D. N.; Wang, Y. C.; Wang, Y.; Wang, R. M.; Ng, K. M.; Naranmandura, H.; Tse, E. W. C.; Sun, H. Z. Arsenic trioxide targets Hsp60, triggering degradation of p53 and survivin. *Chem. Sci.* **2021**, *12* (32), 10893−10900.
(24) Spuches, A. M.; Kruszyna, H. G.; Rich, A. M.; Wilcox, D. E. Thermodynamics of the As(III)-thiol interaction: Arsenite and monomethylarsenite complexes with glutathione, dihydrolipoic acid, and other thiol ligands. *Inorg. Chem.* **2005**, *44* (8), 2964−2972.
(25) Huang, C. S.; Jia, T.; Tang, M. F.; Yin, Q.; Zhu, W. P.; Zhang, C.; Yang, Y.; Jia, N. Q.; Xu, Y. F.; Qian, X. H. Selective and Ratiometric Fluorescent Trapping and Quantification of Protein Vicinal Dithiols and in Situ Dynamic Tracing in Living Cells. *J. Am. Chem. Soc.* **2014**, *136* (40), 14237−14244.
(26) Sapra, A.; Ramadan, D.; Thorpe, C. Multivalency in the Inhibition of Oxidative Protein Folding by Arsenic(III) Species. *Biochemistry-Us* **2015**, *54* (2), 612−621.
(27) Charoensuk, V.; Gati, W. P.; Weinfeld, M.; Le, X. C. Differential cytotoxic effects of arsenic compounds in human acute promyelocytic leukemia cells. *Toxicol. Appl. Pharmacol.* **2009**, *239* (1), 64−70.
(28) Gleeson, M. P.; Hersey, A.; Montanari, D.; Overington, J. Probing the links between in vitro potency, ADMET and physicochemical parameters. *Nat. Rev. Drug. Discovery* **2011**, *10* (3), 197−208.
(29) Huggins, D. J.; Sherman, W.; Tidor, B. Rational Approaches to Improving Selectivity in Drug Design. *J. Med. Chem.* **2012**, *55* (4), 1424−1444.
(30) Wang, J. Y.; Zhou, S. Q.; Cheng, Y.; Cheng, L.; Qin, Y.; Zhang, Z. F.; Bi, A. W.; Xiang, H. J.; He, X. H.; Tian, X. X.; Liu, W. B.; Zhang, J.; Peng, C.; Zhu, Z. J.; Huang, M.; Li, Y.; Zhuang, G. L.; Tan, L. Selective Covalent Targeting of Pyruvate Kinase M2 Using Arsenous Warheads. *J. Med. Chem.* **2023**, *66* (4), 2608−2621.
(31) Baillie, T. A. Targeted Covalent Inhibitors for Drug Design. *Angew. Chem., Int. Ed.* **2016**, *55* (43), 13408−13421.
(32) Lonsdale, R.; Ward, R. A. Structure-based design of targeted covalent inhibitors. *Chem. Soc. Rev.* **2018**, *47* (11), 3816−3830.
(33) Lindvall, J. M.; Blomberg, K. E. M.; Valiaho, J.; Vargas, L.; Heinonen, J. E.; Berglof, A.; Mohamed, A. J.; Nore, B. F.; Vihinen, M.; Smith, C. I. E. Bruton's tyrosine kinase: cell biology, sequence conservation, mutation spectrum, siRNA modifications, and expression profiling. *Immunol. Rev.* **2005**, *203*, 200−215.
(34) Buggy, J. J.; Elias, L. Bruton Tyrosine Kinase (BTK) and Its Role in B-cell Malignancy. *Int. Rev. Immunol.* **2012**, *31* (2), 119−132.
(35) Pan, Z. Y.; Scheerens, H.; Li, S. J.; Schultz, B. E.; Sprengeler, P. A.; Burrill, L. C.; Mendonca, R. V.; Sweeney, M. D.; Scott, K. C. K.; Grothaus, P. G.; Jeffery, D. A.; Spoerke, J. M.; Honigberg, L. A.; Young, P. R.; Dalrymple, S. A.; Palmer, J. T. Discovery of selective irreversible inhibitors for Bruton's tyrosine kinase. *Chemmedchem* **2007**, *2* (1), 58−61.
(36) Hendriks, R. W.; Yuvaraj, S.; Kil, L. P. Targeting Bruton's tyrosine kinase in B cell malignancies. *Nat. Rev. Cancer* **2014**, *14* (4), 219−232.
(37) Herman, S. E. M.; Gordon, A. L.; Hertlein, E.; Ramanunni, A.; Zhang, X. L.; Jaglowski, S.; Flynn, J.; Jones, J.; Blum, K. A.; Buggy, J. J.; Hamdy, A.; Johnson, A. J.; Byrd, J. C. Bruton tyrosine kinase represents a promising therapeutic target for treatment of chronic lymphocytic leukemia and is effectively targeted by PCI-32765. *Blood* **2011**, *117* (23), 6287−6296.
(38) Wang, M. L.; Rule, S.; Martin, P.; Goy, A.; Auer, R.; Kahl, B. S.; Jurczak, W.; Advani, R. H.; Romaguera, J. E.; Williams, M. E.; Barrientos, J. C.; Chmielowska, E.; Radford, J.; Stilgenbauer, S.; Dreyling, M.; Jedrzejczak, W. W.; Johnson, P.; Spurgeon, S. E.; Li, L.; Zhang, L.; Newberry, K.; Ou, Z. S.; Cheng, N.; Fang, B. L.; McGreivy, J.; Clow, F.; Buggy, J. J.; Chang, B. Y.; Beaupre, D. M.; Kunkel, L. A.; Blum, K. A. Targeting BTK with Ibrutinib in Relapsed or Refractory Mantle-Cell Lymphoma. *N. Engl. J. Med.* **2013**, *369* (6), 507−516.
(39) Voice, A. T.; Tresadern, G.; Twidale, R. M.; van Vlijmen, H.; Mulholland, A. J. Mechanism of covalent binding of ibrutinib to Bruton's tyrosine kinase revealed by QM/MM calculations. *Chem. Sci.* **2021**, *12* (15), 5511−5516.
(40) Griffin, B. A.; Adams, S. R.; Tsien, R. Y. Specific covalent labeling of recombinant protein molecules inside live cells. *Science* **1998**, *281* (5374), 269−272.
(41) Yan, X.; Zhang, H.; Wang, Z.; Peng, H.; Tao, J.; Li, X. F.; Le, X. C. Quantitative synthesis of protein-DNA conjugates with 1:1 stoichiometry. *Chem. Commun.* **2018**, *54* (54), 7491−7494.
(42) Nicholson, B. K.; Wilson, P. S.; Nancekivell, A. A re-investigation of arsenoacetic acid, $(AsCH_2COOH)_n$. *J. Organomet. Chem.* **2013**, *745*, 80−85.
(43) Lacoste, A. M.; Dumora, C.; Ali, B. R. S.; Neuzil, E.; Dixon, H. B. F. Utilization of 2-Aminoethylarsonic Acid in Pseudomonas-Aeruginosa. *J. Gen. Microbiol.* **1992**, *138*, 1283−1287.
(44) Brown, S. B.; Turner, R. J.; Roche, R. S.; Stevenson, K. J. Spectroscopic Characterization of Thioredoxin Covalently Modified with Monofunctional Organoarsenical Reagents. *Biochemistry-Us* **1987**, *26* (3), 863−871.
(45) Lloyd, N. C.; Morgan, H. W.; Nicholson, B. K.; Ronimus, R. S. Substituted phenylarsonic acids; structures and spectroscopy. *J. Organomet. Chem.* **2008**, *693* (14), 2443−2450.
(46) Liang, X. F.; Drueckhammer, D. G. Arsinous acid as a thiol binding group: potential cysteine peptide tagging functionality that binds a single thiol. *N. J. Chem.* **2014**, *38* (4), 1368−1371.
(47) Dixon, H. B. F. The biochemical action of arsonic acids especially as phosphate analogues. *Adv. Inorg. Chem.* **1996**, *44*, 191−227.
(48) Prashad, M.; Lu, S.; Kim, H. Y.; Hu, B.; Repic, O.; Blacklock, T. J. An improved and practical sharpless oxidation of primary alcohols to the carboxylic acids. *Synth. Commun.* **1999**, *29* (17), 2937−2942.
(49) Honigberg, L. A.; Smith, A. M.; Sirisawad, M.; Verner, E.; Loury, D.; Chang, B.; Li, S.; Pan, Z. Y.; Thamm, D. H.; Miller, R. A.; Buggy, J. J. The Bruton tyrosine kinase inhibitor PCI-32765 blocks B-

https://doi.org/10.1021/acs.jmedchem.3c02076
J. Med. Chem. 2024, 67, 5458−5472

cell activation and is efficacious in models of autoimmune disease and B-cell malignancy. *P. Natl. Acad. Sci. U.S.A.* **2010**, *107* (29), 13075−13080.
(50) Bender, A. T.; Gardberg, A.; Pereira, A.; Johnson, T.; Wu, Y.; Grenningloh, R.; Head, J.; Morandi, F.; Haselmayer, P.; Liu-Bujalski, L. Ability of Bruton's Tyrosine Kinase Inhibitors to Sequester Y551 and Prevent Phosphorylation Determines Potency for Inhibition of Fc Receptor but not B-Cell Receptor Signaling. *Mol. Pharmacol.* **2017**, *91* (3), 208−219.
(51) Woyach, J. A.; Johnson, A. J.; Byrd, J. C. The B-cell receptor signaling pathway as a therapeutic target in CLL. *Blood* **2012**, *120* (6), 1175−84.
(52) Liang, Q.; Chen, Y.; Yu, K.; Chen, C.; Zhang, S.; Wang, A.; Wang, W.; Wu, H.; Liu, X.; Wang, B.; Wang, L.; Hu, Z.; Wang, W.; Ren, T.; Zhang, S.; Liu, Q.; Yun, C. H.; Liu, J. Discovery of N-(3-(5-((3-acrylamido-4-(morpholine-4-carbonyl)phenyl)amino)-1-methyl-6-oxo-1,6-dihydropyridin-3-yl)-2-methylphenyl)-4-(tert-butyl)-benzamide (CHMFL-BTK-01) as a highly selective irreversible Bruton's tyrosine kinase (BTK) inhibitor. *Eur. J. Med. Chem.* **2017**, *131*, 107−125.
(53) Li, Y. Q.; Lannigan, W. G.; Davoodi, S.; Daryaee, F.; Corrionero, A.; Alfonso, P.; Rodriguez-Santamaria, J. A.; Wang, N.; Haley, J. D.; Tonge, P. J. Discovery of Novel Bruton's Tyrosine Kinase PROTACs with Enhanced Selectivity and Cellular Efficacy. *J. Med. Chem.* **2023**, *66* (11), 7454−7474.
(54) Guo, Y.; Pan, W.; Liu, S.; Shen, Z.; Xu, Y.; Hu, L. ERK/MAPK signalling pathway and tumorigenesis. *Exp. Ther. Med.* **2020**, *19* (3), 1997−2007.
(55) Yan, X. W.; Yang, L. M.; Wang, Q. Q. Lanthanide-Coded Protease-Specific Peptide-Nanoparticle Probes for a Label-Free Multiplex Protease Assay Using Element Mass Spectrometry: A Proof-of-Concept Study. *Angew. Chem., Int. Ed.* **2011**, *50* (22), 5130−5133.
(56) Yan, X. W.; Luo, Y. C.; Zhang, Z. B.; Li, Z. X.; Luo, Q.; Yang, L. M.; Zhang, B.; Chen, H. F.; Bai, P. M.; Wang, Q. Q. Europium-Labeled Activity-Based Probe through Click Chemistry: Absolute Serine Protease Quantification Using 153Eu Isotope Dilution ICP/MS. *Angew. Chem., Int. Ed.* **2012**, *51* (14), 3358−3363.
(57) Yan, X. W.; Yang, L. M.; Wang, Q. Q. Detection and quantification of proteins and cells by use of elemental mass spectrometry: progress and challenges. *Anal. Bioanal. Chem.* **2013**, *405* (17), 5663−5670.
(58) Bradshaw, J. M.; McFarland, J. M.; Paavilainen, V. O.; Bisconte, A.; Tam, D.; Phan, V. T.; Romanov, S.; Finkle, D.; Shu, J.; Patel, V.; Ton, T.; Li, X. Y.; Loughhead, D. G.; Nunn, P. A.; Karr, D. E.; Gerritsen, M. E.; Funk, J. O.; Owens, T. D.; Verner, E.; Brameld, K. A.; Hill, R. J.; Goldstein, D. M.; Taunton, J. Prolonged and tunable residence time using reversible covalent kinase inhibitors. *Nat. Chem. Biol.* **2015**, *11* (7), 525−539.
(59) Serafimova, I. M.; Pufall, M. A.; Krishnan, S.; Duda, K.; Cohen, M. S.; Maglathlin, R. L.; McFarland, J. M.; Miller, R. M.; Frodin, M.; Taunton, J. Reversible targeting of noncatalytic cysteines with chemically tuned electrophiles. *Nat. Chem. Biol.* **2012**, *8* (5), 471−476.
(60) Lanning, B. R.; Whitby, L. R.; Dix, M. M.; Douhan, J.; Gilbert, A. M.; Hett, E. C.; Johnson, T. O.; Joslyn, C.; Kath, J. C.; Niessen, S.; Roberts, L. R.; Schnute, M. E.; Wang, C.; Hulce, J. J.; Wei, B.; Whiteley, L. O.; Hayward, M. M.; Cravatt, B. F. A road map to evaluate the proteome-wide selectivity of covalent kinase inhibitors. *Nat. Chem. Biol.* **2014**, *10* (9), 760−767.
(61) Kiely-Collins, H.; Winter, G. E.; Bernardes, G. J. L. The role of reversible and irreversible covalent chemistry in targeted protein degradation. *Cell Chem. Biol.* **2021**, *28* (7), 952−968.
(62) Degorce, S. L.; Anjum, R.; Dillman, K. S.; Drew, L.; Groombridge, S. D.; Halsall, C. T.; Lenz, E. M.; Lindsay, N. A.; Mayo, M. F.; Pink, J. H.; Robb, G. R.; Scott, J. S.; Stokes, S.; Xue, Y. F. Optimization of permeability in a series of pyrrolotriazine inhibitors of IRAK4. *Bioorgan. Med. Chem.* **2018**, *26* (4), 913−924.
(63) Faust, A.; Bäumer, N.; Schlütermann, A.; Becht, M.; Greune, L.; Geyer, C.; Rüter, C.; Margeta, R.; Wittmann, L.; Dersch, P.; Lenz, G.; Berdel, W. E.; Bäumer, S. Tumor-Cell-Specific Targeting of Ibrutinib: Introducing Electrostatic Antibody-Inhibitor Conjugates (AiCs). *Angew. Chem., Int. Ed.* **2022**, *61* (1), No. e202109769.
(64) Cullen, W. R.; Liu, Q. Q.; Lu, X. F.; McKnight-Whitford, A.; Peng, H. Y.; Popowich, A.; Yan, X. W.; Zhang, Q.; Fricke, M.; Sun, H. S.; Le, X. C. Methylated and thiolated arsenic species for environmental and health research - A review on synthesis and characterization. *J. Environ. Sci.* **2016**, *49*, 7−27.
(65) Bianco, G.; Forli, S.; Goodsell, D. S.; Olson, A. J. Covalent docking using autodock: Two-point attractor and flexible side chain methods. *Protein Sci.* **2016**, *25* (1), 295−301.

https://doi.org/10.1021/acs.jmedchem.3c02076
J. Med. Chem. 2024, 67, 5458−5472